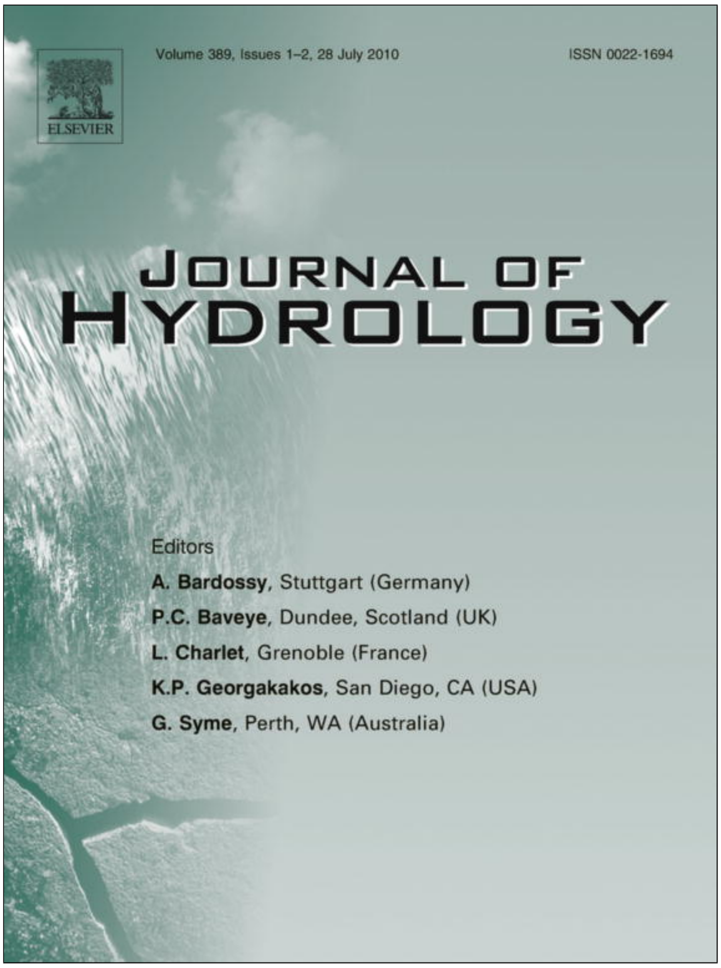
Volume 389, Issues 1–2, 28 July 2010
ISSN 0022-1694
ELSEVIER
JOURNAL OF
HYDROLOGY
Editors
A. Bardossy, Stuttgart (Germany)
P.C. Baveye, Dundee, Scotland (UK)
L. Charlet, Grenoble (France)
K.P. Georgakakos, San Diego, CA (USA)
G. Syme, Perth, WA (Australia)

Journal of Hydrology 389 (2010) 1–17

Contents lists available at ScienceDirect

Journal of Hydrology

journal homepage: www.elsevier.com/locate/jhydrol

Hydrogeology of the south-eastern Yucatan Peninsula: New insights from water level measurements, geochemistry, geophysics and remote sensing

Bibi R.N. Gondwe [a,*], Sara Lerer [a], Simon Stisen [b], Luis Marín [c], Mario Rebolledo-Vieyra [d], Gonzalo Merediz-Alonso [e], Peter Bauer-Gottwein [a]

[a] Department of Environmental Engineering, Technical University of Denmark, Miljoevej, Building 113, DK-2800 Kgs. Lyngby, Denmark
[b] Geological Survey of Denmark and Greenland (GEUS), Oester Voldgade 10, DK-1350 Copenhagen, Denmark
[c] Instituto de Geofísica, Universidad Nacinal Autónoma de México, Cd. Universitaria, México DF 04510, Mexico
[d] Centro para el Estudio del Agua, CICY-Quintana Roo, Calle 8, Lote 1, No. 39, Manzana 20 SM 64, Cancún, Quintana Roo 77500, Mexico
[e] Amigos de Sian Ka'an, Calle Fuego No. 2, Manzana 10 SM 4, Cancún, Quintana Roo 77500, Mexico

A R T I C L E   I N F O

Article history:
Received 12 October 2009
Received in revised form 10 February 2010
Accepted 29 April 2010

This manuscript was handled by P. Baveye, Editor-in-Chief, with the assistance of Barbara J. Mahler, Associate Editor

Keywords:
Conceptual model
Karst
Aquifer
Sian Ka'an
Mexico

S U M M A R Y

The Yucatan Peninsula is one of the world's largest karstic aquifer systems. It is the sole freshwater source for human users and ecosystems. The region hosts internationally important groundwater-dependent ecosystems (GDEs) in the 5280 km^2 Sian Ka'an Biosphere Reserve. The GDEs are threatened by increasing groundwater abstractions and risks of pollution. Hydrogeological exploration work is needed as basis for sound groundwater management. A multidisciplinary approach was used to study this data-scarce region. Geochemical data and phreatic surface measurements showed distinct hydrogeological units in the groundwater catchment of Sian Ka'an. The hilly southwestern areas had a low hydraulic permeability, likely caused by a geology containing gypsum, whereas the transition zone and flat areas in the east and north had a high permeability. In the latter areas, the fresh groundwater could be described by a Dupuit–Ghyben–Herzberg lens. Geophysical borehole logging and time-domain electromagnetic soundings identified a shallow, low-resistive and high-gamma-radiation layer present throughout the hilly area and transition zone. Its thickness was 3–8 m, apparent conductivity was 200–800 mS/m and natural gamma-radiation about 80 counts pr. second. The layer is proposed to be ejecta from the Chicxulub impact (Cretaceous/Paleogene boundary). Spatial estimates of recharge were calculated from MODIS imagery using the 'triangle method'. Average recharge constituted 17% of mean annual precipitation in the study area. Recharge was greatest in the hilly area and towards Valladolid. Near the coast, average actual evapotranspiration exceeded annual precipitation. The multidisciplinary approach used in this study is applicable to other catchment-scale studies.

1. Introduction

Globally, groundwater-dependent terrestrial ecosystems are receiving increased attention due to growing recognition that water must be available for ecosystems as well as for people (Eamus and Froend, 2006; Münch and Conrad, 2007; Krause et al., 2007). Groundwater-dependent ecosystems (GDEs) in karst environments are recognized as important ecosystems, and are the target of restoration and protection efforts (Wolfe, 1996; Loftus et al., 2001; Kilroy et al., 2005; Mazzotti et al., 2005). These ecosystems are extremely vulnerable to pollution due to the rapid infiltration, the fast water flow through caves and the limited retention of contaminants in karst geology.

One of Mexico's largest protected areas, the 5280 km^2 Sian Ka'an Biosphere Reserve, is a groundwater-dependent ecosystem in karst. Located in the eastern part of the Yucatan Peninsula, it hosts vast wetlands, fed by groundwater, taking up roughly ⅓ of the reserve. These wetlands are internationally valued and listed as UNESCO World Heritage and a Ramsar site (http://whc.unesco.org/en/list; www.ramsar.org). Their diverse ecosystems and recreational value make them important for the region. Their groundwater source is a thin freshwater lens, only up to 100 m thick. Effectively it is the only fresh water resource available for human use and ecosystems on the Yucatan Peninsula.

On the Peninsula, water demands are growing, along with threats from pollution. Escolero et al. (2000) and Pacheco et al. (2001) documented groundwater pollution problems and significant water abstraction in the north-western Yucatan Peninsula.

* Corresponding author. Tel.: +45 4525 1570; fax: +45 4593 2850.
E-mail addresses: bng@env.dtu.dk (B.R.N. Gondwe), sst@geus.dk (S. Stisen), lmarin@geofisica.unam.mx (L. Marín), marior@cicy.mx (M. Rebolledo-Vieyra), gmerediz@amigosdesiankaan.org (G. Merediz-Alonso), pbg@env.dtu.dk (P. Bauer-Gottwein).

0022-1694/$ - see front matter © 2010 Elsevier B.V. All rights reserved.
doi:10.1016/j.jhydrol.2010.04.044

Along the eastern coast the tourism industry is expanding, which leads to a rapid increase in population density and water demands (Fideicomiso, 2004). Agricultural activities are intensifying (Mazzotti et al., 2005). Wastewater treatment in the region is poorly implemented. Typically, wastewater is re-injected into the aquifer (ASK, 2003; Marín et al., 2000; Krekeler et al., 2007). Trading off ecosystem water use and human water use emerges as one of the major groundwater management problems on the Yucatan Peninsula.

For sound management of groundwater-dependent ecosystems, a catchment-scale focus is important. However, delineating catchments in karst poses a challenge, due to the complex and heterogeneous nature of karst aquifers. Comprehensive hydrogeologic datasets are required for this purpose. Hydrogeological data are generally scarce in the (south)eastern part of the Yucatan Peninsula. Existing data on the region primarily concentrate on the State of Yucatan, the Cancun area in northern Quintana Roo and the Riviera Maya (e.g. González-Herrera et al., 2002; Graniel et al., 1999; Marín, 1990; Méndez Ramos, 1991; Moore et al., 1992; Beddows, 2004; Steinich and Marín, 1996, 1997; Back and Hanshaw, 1970; Lesser, 1976; Hanshaw and Back, 1980). Only Perry et al. (2002, 2009) and Kenkmann and Schönian (2006) reported geologic and hydrogeologic aspects for the central and south-eastern parts of the Peninsula. They indicated that the (hydro)geology here is different from that in Yucatan State, due to the occurrence of an incompletely mapped ejecta layer originating from the late Cretaceous Chicxulub meteorite impact (Hildebrand et al., 1991; Pope et al., 1991). The presence of lakes and seasonally inundated forests and swamps in southern Quintana Roo also indicates a hydrogeology different from the highly permeable geology of the northern part of the Peninsula. With the pressure to further develop tourism activities north and south of the Sian Ka'an Biosphere Reserve, it is important to develop a quantitative understanding of the regional hydrology. Groundwater flow patterns towards Sian Ka'an need to be established. Without knowing where catchment boundaries and main recharge zones are located, management and preservation of these unique wetlands is difficult.

To develop a quantitative hydrogeological understanding of Sian Ka'an's catchment, this study uses a multidisciplinary approach. Geophysical, remotely sensed, water chemical and water level surveys are combined and identify important hydrogeologic differences between the flat and hilly parts of the catchment. Groundwater recharge in the catchment is quantified and its spatial distribution is mapped. A shallow layer of low permeability in parts of the catchment is mapped comprehensively for the first time, and is proposed to be ejecta from the Chicxulub meteorite impact. The collected hydrogeologic data are then combined into a consistent conceptual model of the karstic groundwater catchment of Sian Ka'an.

2. Methods and data

2.1. The study area

The study area is the tentative groundwater catchment of the Sian Ka'an Biosphere Reserve, located in Quintana Roo, Mexico (Fig. 1). The study area was delineated based on topographic divides, assuming, as a first order approximation, that these divides coincide with groundwater divides. The groundwater head data presently available for the Peninsula are in agreement with these boundaries. Geochemical findings of Perry et al. (2002) support the water divide location at Lake Chichankanab.

Average precipitation ranges from 840 to 1550 mm/year. Three quarters of the precipitation falls between May and October (unpubl. climate data from Comisión Nacional del Agua (CONAGUA)). Actual evapotranspiration is poorly estimated; estimates range from 40% to 85% of mean annual precipitation (Lesser, 1976; Beddows, 2004). Average monthly temperatures range from 23 to 27 °C. The area is subject to tropical storms. Soil cover is limited and most of the area is covered by 15–30 m tall semi-evergreen forest (Sánchez-Sánchez and Islebe, 2002; INEGI, 1997. Sian Ka'an contains coastal savannas, swamps, marches and mangrove, in addition to tropical forests, and hosts endangered and endemic species (Morales Barbosa, 1992; Mazzotti et al., 2005). From August 2006 to February 2008 the wetland extent varied between 1067 and 2588 km^2. Smallest extent was in May and largest in December in a typical year (Gondwe et al., 2010).

The study area contains a notable topographic contrast. The topographic relief is flat in the northern and coastal part (elevations 0–20 m above mean sea level (mamsl)), whereas the south–southwestern areas have an undulating relief with cone-karst landforms (elevations 50–340 mamsl). In between is a transition zone with moderately undulating relief (20–50 mamsl). These areas are called the flat area, the hilly area, and the transition zone in the remainder of this paper (Fig. 6b). Depressions forming seasonal swamps ('bajos', 'poljes') are found in the hilly area (Pope and Dahlin, 1989; Gunn et al., 2002; Tun-Dzul et al., 2008; Beach et al., 2008). Seasonal surface drainage connects some of these swamps (Fig. 1; SGM, 2007) yet not all ephemeral streams appear to have been officially mapped. No perennial rivers are present within the study area, but the majority of the Peninsula's relatively few lakes are found in the centre of the study area. In contrast, no lakes are present in the northern Peninsula. The only surface water bodies in the north are sinkholes ('cenotes'). Cenotes are also present throughout the study area, most abundantly in the flat area and transition zone. The total number of cenotes on the Peninsula is unknown but exceeds 1000.

Previous studies have established significant seawater intrusion into the aquifer for the Yucatan State and Riviera Maya (Back and Hanshaw, 1970; Perry et al., 1989, 1995; Steinich and Marín, 1996; Moore et al., 1992; Beddows, 2004; Beddows et al., 2007). In Yucatan State the saltwater has been detected up to ~90 km inland (Back and Hanshaw, 1970; Steinich and Marín, 1996), whereas only the near-coastal zone has been studied in Quintana Roo. Groundwater levels referenced to mean sea level have only been mapped in Yucatan State (Marín, 1990).

2.2. Geological framework

The Yucatan Peninsula consists of limestones, dolomites and evaporites reaching thicknesses of >1500 m (Weidie, 1985). The sediments exposed at the ground surface spans Upper Cretaceous to Holocene in age, and are generally nearly horizontally layered and off-lapping, with gradually younger carbonates deposited towards the Peninsula margins (Lopez-Ramos, 1975; SGM, 2007; Schönian et al., 2005). The Cretaceous age of the oldest sediments exposed at the ground surface is a recent interpretation (Schönian et al., 2005) but the possibility was already mentioned by Lesser (1976). The age of the sediments exposed at the ground surface will be used to refer to various parts of the study area (e.g. Pliocene area) in the remainder of this paper. Kenkmann and Schönian (2006) emphasized that the geology of the southern Peninsula is poorly constrained due to few exposures and difficulties in dating the sediments through biostratigraphy. The Yucatecan carbonates are heavily karstified. They host abundant caves, including the world's longest underwater cave system (http://www.caves.org/project/qrss/qrlong.htm; http://www.caverbob.com/uwcave.htm). Mapped caves are mainly found on the Riviera Maya; possibly as a result of its vicinity to population centers, rather than lack of cave systems inland (Smart et al., 2006; Beddows, 2004). Regional-scale

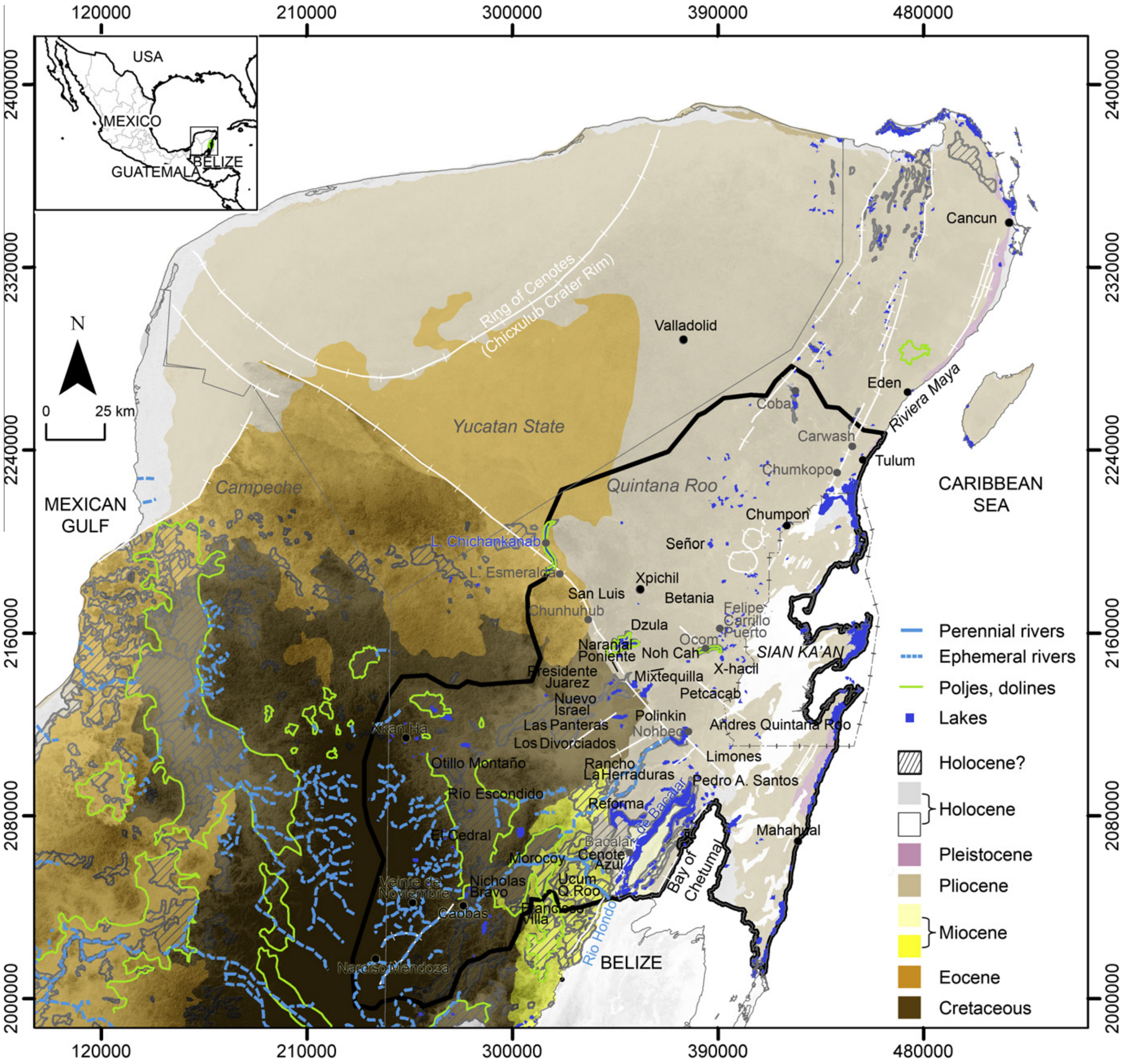

Fig. 1. Geology of the Yucatan Peninsula, modified from SGM (2007). Oldest sediments dated as Cretaceous instead of Paleocene, based on Schönian et al. (2005) and Lopez-Ramos (1975) (Ichaiche Formation). Topography from SRTM (USGS, 2006) overlain as grey-scaled transparent. Study area outlined with thick grey polygon. Coordinates are UTM zone 16 N, WGS84 datum and ellipsoid.

zones of higher permeability were investigated in Gondwe et al. (submitted for publication).

Ejecta associated with the Chicxulub meteorite impact, at the contact between Cretaceous and Paleogene sediments, have been found in southern Quintana Roo and neighboring Belize (Ocampo et al., 1996; Fouke et al., 2002; Pope et al., 2005; Schönian et al., 2005; Kenkmann and Schönian, 2006). The Chicxulub impact occurred in the north-western Yucatan Peninsula (Hildebrand et al., 1991; Pope et al., 1991), 80–350 km from the study area. The extent of the possible ejecta blanket in the study area is not well known. Based on geochemical data Perry et al. (2009) proposed that the ejecta blanket extends south and east of Lake Chichankanab. It appears that in official geological maps some ejecta deposits in the hilly region may have been misdated to be Quaternary deposits, as some locations correlate with locations mapped by Kenkmann and Schönian (2006) as ejecta (Neuman and Rahbek, 2007; Perry et al., 2009). The ejecta is expected to have a low hydraulic permeability, as it is clay-rich, and described to have a sealing or partially sealing effect (Ocampo et al., 1996; Grajales-Nishimura et al., 2000; Perry et al., 2009).

2.3. Water level measurements

Static groundwater levels were measured at 89 hand-dug and drilled wells within the study area. Surface water levels were measured at 12 locations in wetlands and permanent lakes near Sian Ka'an, and at 2 locations in the hilly area. Water levels were referenced to EGM96 mean sea level using static carrier phase GPS. Data processing was carried out in the Trimble Total Control software (Trimble, 2003) using IGS final ephemeris from http://www.igscb.jpl.nasa.gov/components/prods_cb.html. Estimated uncertainty on the z-coordinate was ±1–7 cm (absolute average:

4 cm), based on reoccupation of 7 rover points. Four water level measurement campaigns were carried out; two in the dry season (February–April 2007, February 2008), one in the early wet season (July 2007) and one in the late wet season (November–December 2008). Not all 103 locations were measured in each campaign. Water level measurements were carried out to the nearest cm from marked geo-referenced points, yielding an uncertainty of ±0.5 cm on temporal water level variations. At three different locations Schlumberger Mini-Diver pressure transducers were employed to measure temporal water level variation in detail. Measurements were compensated for barometric changes measured with Schlumberger Baro-Divers. Uncertainty on Mini-Diver measurements were ±5 mm.

2.4. Geophysical measurements

Twenty-one time-domain electromagnetic measurements (TEM) were carried out to investigate geology and map the depth to the freshwater–saltwater interface – the halocline. The flat area and transition zone were sampled representatively, whereas the hilly part was not sampled, due to time constraints. A ProTEM47 instrument (Geonics Ltd., Canada) with a 40×40 m^2 transmitter coil in central loop configuration was employed. Repetition frequencies of 285 Hz (1 A current), 75 Hz and 30 Hz (both 3 A current) were used. Decay of the secondary magnetic field was sampled in 20 time gates covering 35 µs to 7 ms after end of current turn-off ramp. Data processing and least squares 1D layered inversion was carried out with the SiTEM-SEMDI software (HGG, Denmark, 2001, 2007; Munkholm and Auken, 1996; Effersø et al., 1999). For each sounding location the inversion result with best compromise between model simplicity and model fit was chosen. The ability of the TEM method to detect depths to the halocline depends on local geologic conditions and goodness-of-fit of the inversion to data. In a previous study, the depth to halocline obtained from TEM was within 5 m of that observed in boreholes (Goldman et al., 1991). Elevations from Shuttle Radar Topography Mission (SRTM) data (USGS, 2006) were used to convert depths to elevation (mamsl), as elevations determined by GPS were not available for the TEM sites. Error bars given by the inversion routine were added 5 m in each direction to compensate for possible SRTM error (typically e.g. 4–9 m according to Kocak et al. (2005), Gorohkhovich and Voustianiouk (2006), and Weydahl et al. (2007)).

Geophysical borehole logging was carried out at 17 sites, mostly wells belonging to private ranches. Fluid temperature and fluid specific electrical conductivity (SEC) was carried out with a Solinst 107 Temperature Level Conductivity meter. Electromagnetic induction log was carried out with an EM39 probe, and natural gamma logging with a GAMMA39 probe (both Geonics Ltd., Canada). Reported induction log results have been adjusted according to the calibration curve given in McNeill (1986). Gamma logs were repeated at least two times to obtain a more certain determination of the highly variable natural gamma-radiation. Repetitions were essentially equal. At one site (Presidente Juarez) an induction log could not be carried out due to metal well casing. All other well casings were PVC.

2.5. Water chemistry

Twenty-eight groundwater samples were taken from actively pumping municipal wells, after pumping out at least 1 m^3 of water through the hose to avoid stagnant water. Three surface water samples were obtained as grab samples at locations with active flow of water. At Cenote Azul water 0.5 m below the surface was sampled. Samples were filtered in the field through 0.45 µm filters, and stored in air-tight PE bottles. Bottles for cation analysis had been acid-rinsed in 5% nitric acid, and were stored full of deionized water, which was decanted immediately prior to each sampling. Bottles were rinsed with sample water before being filled. After filling it was ensured that there was no headspace. Separate bottles for alkalinity, cation and anion analysis were used. Samples for alkalinity and sulfate were stored in an ice cooler after sampling, and refrigerated at 5 °C until analysis. Alkalinity was determined 8–28 days after sampling by titration to pH 4.5 using 1.6 N H_2SO_4 acid and a Hach digital titrator following APHA (1998a). Expected precision is approx. ±1 mg $CaCO_3$/L. Sulfate was determined 7–27 days after sampling using the turbidimetric method (APHA, 1998b), with precision of approx. ±0.3 meq SO_4/L, based on repeatability test. Remaining samples were transported by air and stored frozen until analysis. For cations, samples were stabilized with concentrated HNO_3 (concentration in sample: 1% v/v), and left for two weeks at 5 °C before analysis to ensure dissolution of any precipitated carbonate. Cations were analyzed on a Varian Vista MPX Axial View Inductively Coupled Plasma Optical Emission Spectrometer (ICP-OES). Three replicates were run, and one was spiked with all the cations for control. Anions, except sulfate, were analyzed on a Dionex ion chromatograph ICS-1500 with an AMMS anion suppressor. Analytical precision ranged at or below ±7% for cations, ±5% for anions.

The PHREEQC software (Parkhurst and Appelo, 1999) was used to calculate mineral saturation indices. Since pH and temperature had not been measured in the field, most recent values available from Comisión de Agua Potable y Alcantarillado (CAPA) (unpubl. data) measured for the same wells were used. Where no values were available from CAPA or Perry et al. (2002), an average of the values for the other localities was used (pH: 7.3, temperature: 28.5 °C). Equilibrium constants from the database phreeqc.dat were used. Measured alkalinity was assumed equal to the HCO_3-concentration, since at the samples' pH values the contribution from other anions to alkalinity can be neglected.

2.6. Remote sensing

2.6.1. Soil water balance

The water balance equation for the soil zone in the catchment can be written as:

$$\frac{dV}{dt} = P - ET_a - Q - R \tag{1}$$

where V: volume of water stored in the soil zone (e.g. mm), dt: change in time (e.g. year), P: precipitation rate, ET_a: actual evapotranspiration rate, Q: rate of surface runoff, R: groundwater recharge rate (all e.g. mm/year). In the present case the recharge rate is equal to the sum of groundwater outflow from the catchment to the coast and the groundwater abstracted. All quantities in Eq. (1) may be a function of space and time. When considering long-term averaged conditions based on several years, the change in volume of water stored in the soil zone over time becomes zero, as storage can be assumed constant. Q can also be assumed zero within the catchment studied, as any (ephemeral) runoff created is expected to infiltrate to the groundwater in a steady-state long-term average scenario. Thus recharge can be estimated as the difference of precipitation and actual evapotranspiration.

2.6.2. Rainfall data

Daily precipitation data were obtained by summing the Tropical Rainfall Measuring Mission (TRMM) 3B42 3-hour precipitation product in the period 2004–2008 (NASDA/NASA, 2008). TRMM product 3B43 was used for monthly precipitation for 1998–2008. Comparison with monthly station data from CONAGUA showed good agreement with respect to timing of rainfall, but showed TRMM estimates to be generally lower than station data. Before use, TRMM data were therefore adjusted to ground truth measurements following Wolff et al. (2005), utilizing monthly data from 23 CONAGUA precipitation stations located in the study area. TRMM spatial resolution is 0.25° × 0.25°.

2.6.3. Evapotranspiration determined from MODIS imagery

Actual evapotranspiration (ET_a) was estimated using the 'triangle method' and the Priestley–Taylor equation, following Jiang and Islam (2001) and Stisen et al. (2008). The Priestley–Taylor equation takes its basis in the Penman–Monteith equation (Monteith, 1965) and defines ET_a as:

$$ET_a = \phi\left[(R_n - G)\frac{\Delta}{\Delta + \gamma}\right] \tag{2}$$

where ET_a is here in (W/m^2), ϕ is the Priestley–Taylor parameter (Priestley and Taylor, 1972) (dimensionless), R_n is net radiation (W/m^2), G is soil heat flux (W/m^2), Δ is the slope of the saturated vapour pressure curve (kPa/K) and γ is the psychrometric constant (kPa/K). ϕ is assumed to represent the aerodynamic term. It is an effective surface resistance to evapotranspiration, not related to a single surface attribute (Jiang and Islam, 1999). ϕ may vary between 0 and $(\Delta + \gamma)/\Delta$, yielding ET_a between 0 and the maximum available energy $(R_n - G)$. The evaporative fraction (EF) (dimensionless), i.e. the amount of energy used on evapotranspiration compared to available energy can be written as:

$$EF = \frac{ET_a}{(R_n - G)} \tag{3}$$

or

$$EF = \phi\left[\frac{\Delta}{\Delta + \gamma}\right] \tag{4}$$

In the 'triangle method' a physical relation is assumed between ϕ and the T_s–VI space. T_s is land surface temperature, VI is a vegetation index. T_s is plotted versus VI for all pixels in the area studied. The plot will show a triangular space. The lower horizontal edge of the triangle ('wet edge', i.e. constant T_s, varying VI) represents potential ET; temperature is reduced to a minimum in these pixels because of maximum evaporative cooling. The upper, slanting, edge of the triangle ('dry edge') represents minimum ET_a for each VI class (cf. Fig. 1 in Stisen et al. (2008)). The position of each pixel in the triangle hence reveals information on its degree of EF. $\phi_{\max}$ is assigned to pixels where T_s is minimum and VI is maximum. $\phi_{\min}$ is assigned to pixels where T_s is maximum and VI is minimum. The VI axis is divided into intervals of equal size. Then ϕ_i of each pixel can be calculated as:

$$\phi_i = \frac{T_{ii,\max} - T_i}{T_{i,\max} - T_{i,\min}} \cdot (\phi_{\max} - \phi_{i,\min}) + \phi_{i,\min} \tag{5}$$

where $T_{i,\max}$ and $T_{i,\min}$ are the maximum and minimum temperatures, respectively, for the VI interval in question, and $\phi_{i,\min}$ is the lower bound of ϕ for each VI interval. $\phi_{i,\min}$ is here established using the relation proposed in Stisen et al. (2008):

$$\phi_{i,\min} = \phi_{\max} \cdot \left[\frac{VI_i - VI_{\min}}{VI_{\max} - VI_{\min}}\right]^2 \tag{6}$$

When ϕ_i is obtained for each pixel, Eqs. (4) and (3) are used to calculate first the EF of each pixel, and next the ET_a of each pixel.

The 'triangle method' requires that minimum and maximum evaporative fractions can be observed in the analyzed area, because both the dry edge and the wet edge of the triangle must be defined by the data. Therefore, the spatial area used for ET_a estimation was the whole Peninsula, so that both the drier north-western Yucatan Peninsula with less dense vegetation, and the more humid study area with more dense vegetation, were included. The period 2004–2008 was covered. As VI the MODIS enhanced vegetation index (EVI) (in the 16-day product MYD13A2) was used, since EVI has a higher sensitivity over dense vegetation, such as the study area, than other often used VIs such as the normalized difference vegetation index (NDVI). Difference in daily day and night land surface temperature was used (dT_s), as this is preferred to using daytime land surface temperature only in the triangle method (Anderson et al., 1997; Wang et al., 2006). The MODIS Aqua product MYD11A1 was used, as these overpass times (approx. 1 am and 1.30 pm local time) were better suited than MODIS Terra's. Spatial resolution of MODIS products was 1 × 1 km^2. To calculate ET_a from evaporative fraction, net radiation (R_n) was calculated as the sum of net shortwave and net longwave radiation obtained from the European Center for Medium-Range Weather Forecast (ECMWF) 12-h accumulated daytime forecast data (Surface Solar Radiation, SSR, ECMWF parameter #176, and Surface Thermal Radiation, STR, ECMWF parameter #177, respectively). Comparison with net radiation measured by automatic climate stations from CONAGUA showed good agreement. ECMFW data products had 0.5° × 0.5° resolution in 2004 and 2005, and 0.25° × 0.25° resolution from 2006 onwards. Soil heat flux, G, was calculated using the empirical relationship of Kustas et al. (1993):

$$G = R_n \cdot (0.40 - 0.33 \cdot \text{NDVI}) \tag{7}$$

Due to cloud cover, ET_a could not be calculated daily for all pixels. Instead, the adjusted crop coefficient ($K_{c_{adj}}$) for the available days was calculated for each pixel (Allen et al., 1998):

$$K_{c_{adj}} = \frac{ET_a}{ET_{ref}} \tag{8}$$

The 'adjusted' term is used when dealing with crops grown under non-standard conditions; see Allen et al. (1998). The reference evapotranspiration (ET_{ref}) needed was calculated with Hargreaves's equation (Hargreaves and Samani, 1985; Allen et al., 1998) for every 10 days using the ECMWF reanalysis data product 2T (2 m temperature, ECMWF parameter #167). Hargreaves' equation was chosen because parameters for using the FAO Penman–Monteith equation were not available. Subsequently, the crop coefficients were interpolated in time following Brunner et al. (2004) to provide temporally variable K_c estimates for all days for all pixels. Finally, daily ET_a could be calculated for the missing days in each pixel by using Eq. (8) and the interpolated daily crop coefficients and reference ET at each pixel.

The root mean square error (RMSE) of the used 'triangle method' was found in Stisen et al. (2008) to be 41.45 W/m^2 = 1.5 mm/day, which is the same order of magnitude as that found by most other authors, cited in Stisen et al. (2008). Recalculating this to the uncertainty on a yearly average estimate by dividing with $\sqrt{365}$ yields an RMSE of 0.08 mm/day (=29 mm/year).

3. Results

3.1. Water levels and water level changes

Water level measurements showed a regional difference in groundwater levels, coinciding with the geological difference in age of the sediments exposed at the ground surface (cf. Figs. 2 and 1). In the Pliocene area, groundwater levels ranged below 3 mamsl whereas groundwater encountered in the Cretaceous geology ranged from about 4 to 260 mamsl. This regional difference was observed during both wet and dry seasons. Water levels indicated that the general groundwater flow direction was SW–NE from the Cretaceous area to the Pliocene area, whereas in the Pliocene area, the groundwater flow direction was W–E towards the coast.

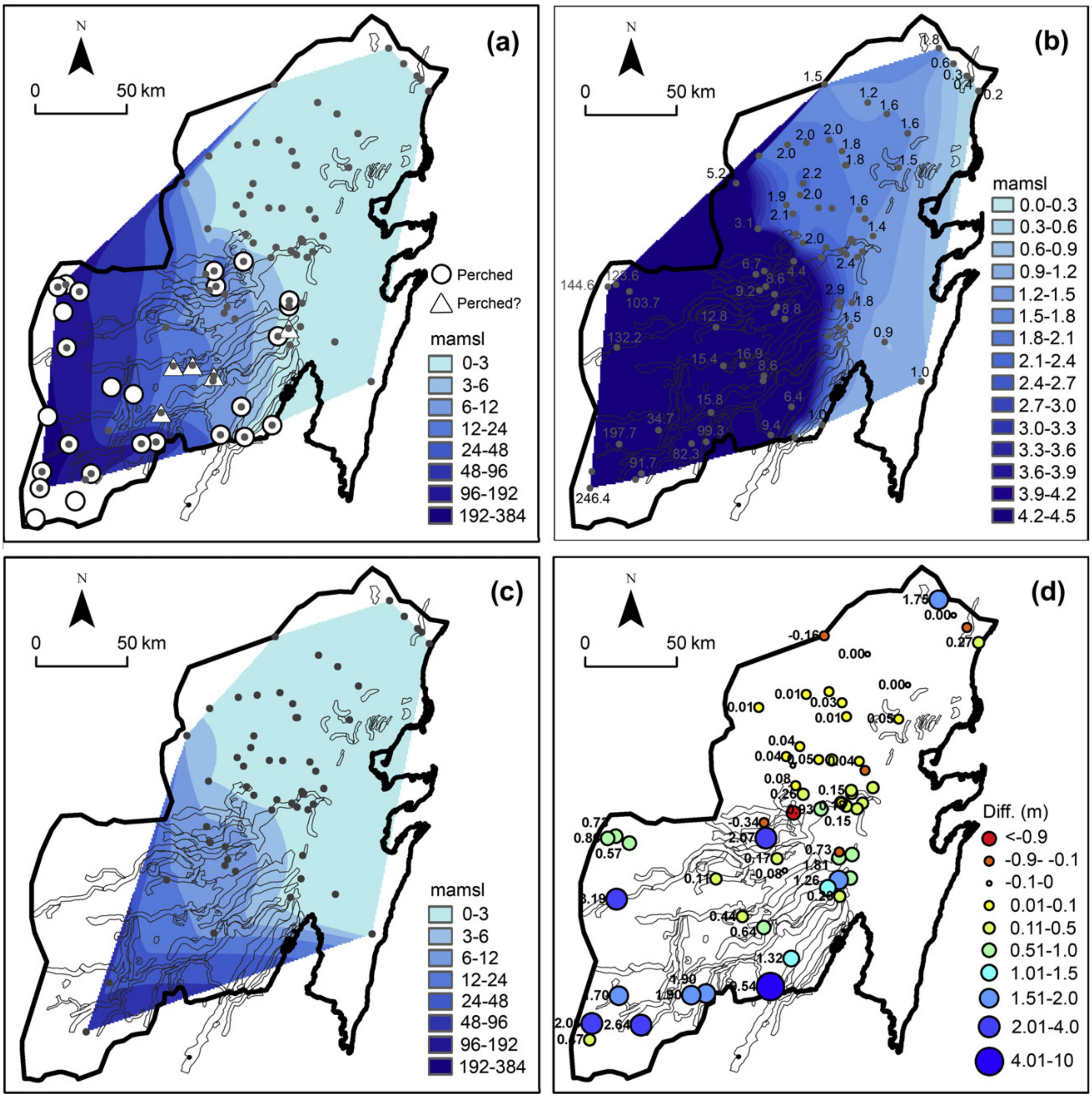

Fig. 2. (a–c) Water levels measured in the dry season (February) 2008, interpolated using Natural Neighbor algorithm. (*a* + *b*) include the points believed to be perched water; (c) excludes these points. The different legends of (a) and (b) are made to more clearly show the overall regional water level differences in the hilly area, and in the flat area, respectively. Water levels refer to meters above mean sea level, and measured values are labeled in (b). The "Perched?" label in (a) indicates localities with possibly perched aquifers. (d) Water level changes between the dry (February) and the wet (November–December) season 2008, given in meters. Positive values indicate an increase in water levels from the dry to the wet season.

A regional difference in the magnitude of temporal water level changes was also seen between the Pliocene and Cretaceous areas. Largest increases between dry and late wet season 2008 were all seen to take place in the Cretaceous geology (20–954 cm) (Fig. 2d). In contrast, no or little change (0–5 cm increases) were generally seen to occur in the Pliocene area (Fig. 2d).

The continuous hydrographs from the locations of Presidente Juarez (Cretaceous area) (Fig. 3a) and Dzula (Pliocene area) (Fig. 3b) were notably different. Whereas Presidente Juarez showed water level variations of about 350 cm within April 2007 to February 2008, Dzula only showed water level variations of approx. 40 cm within July 2007 to February 2008. The Presidente Juarez hydrograph was jagged, and showed many steep changes of e.g. 150 cm within two weeks, whereas the Dzula hydrograph showed smooth transitions. The Petcacab hydrograph (Pliocene area) was short but had the same smooth pattern as the Dzula hydrograph (Fig. 3c). The jagged pattern of Presidente Juarez corresponded very well with times when rainfall events had occurred in the local area (Fig. 3a). Every time a large rainfall event occurred, the water levels reacted instantaneously. At Dzula, increases also took place following a large rainfall event in the local area, but increases occurred more smoothly. The Petcacab hydrograph showed similar behavior. All hydrographs reacted more closely to the rainfall falling in the TRMM pixel in which they were located (approx. 27.5 km $\times$ 26 km), than to the average rainfall falling in the study area (Fig. 3).

Presence of water relatively close to the surface in the Cretaceous geology, and the jagged patterns of the Presidente Juarez

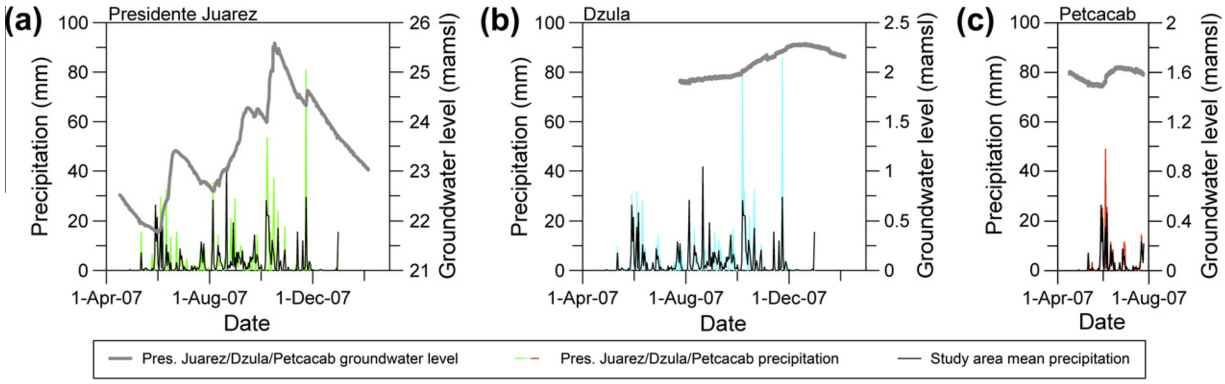

Fig. 3. Hydrographs from (a) Presidente Juarez, (b) Dzula and (c) Petcacab, measured with pressure transducers. Mean daily precipitation in the study area is given in every figure along with daily precipitation over the locality itself. Precipitation derived from TRMM 3B42 3-h product (NASDA/NASA, 2008).

hydrograph, indicated that perched aquifers may be present in parts of the study area. The Cretaceous geology is characterized by generally higher elevations than the other geologies, but, as mentioned, geological boundaries in Fig. 1 are only approximate. Two criteria – ground elevation larger than 30 mamsl (as surrogate for geology) and proximity of water table to ground surface ⩽10 m – were therefore used to map locations which likely have perched aquifers (Fig. 2a). All these locations had large temporal water level changes (mostly >1 m, frequently several meters). That is consistent with having localized perched aquifers, since they would respond more abruptly to precipitation and runoff effects than a regional aquifer in a highly transmissive medium would. Five additional localities had similarly large water level changes, but did only approximately fulfill the two criteria. These locations are marked as 'possibly perched' in Fig. 2a.

When excluding these perched or possibly perched localities the hydraulic gradient in the Cretaceous area was 10–190 cm/km. This is significantly larger than that of the Pliocene area, which had a hydraulic gradient of 3–7 cm/km. This again showed the regional difference between the Pliocene and the Cretaceous areas.

3.2. TEM results

3.2.1. Depth to the halocline

Depth to halocline, determined from inversion of TEM measurements, revealed the expected freshwater lens shape (Fig. 4a). The

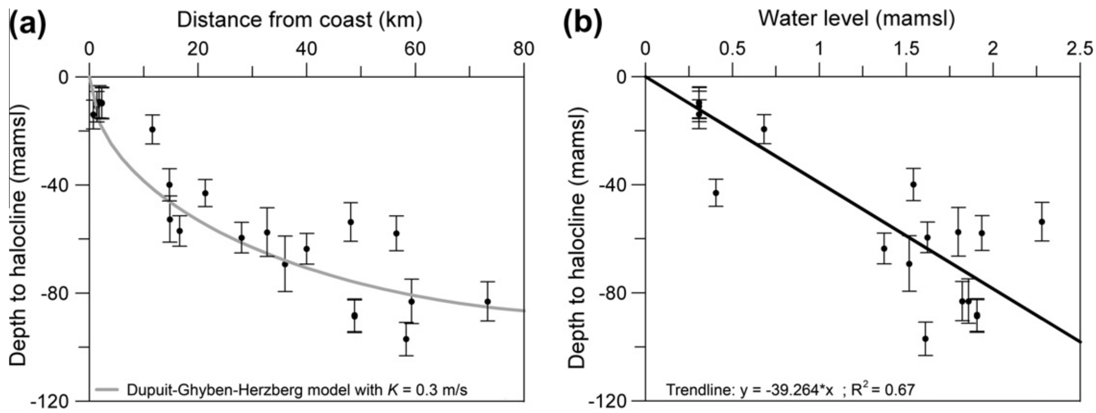

Fig. 4. (a) Depth to halocline measured with TEM as a function of distance from coast. Grey line indicates best fit of the Dupuit–Ghyben–Herzberg model to data. (b) Depth to halocline as a function of measured water levels, both with respect to mean sea level. Best linear regression curve shown as bold black line.

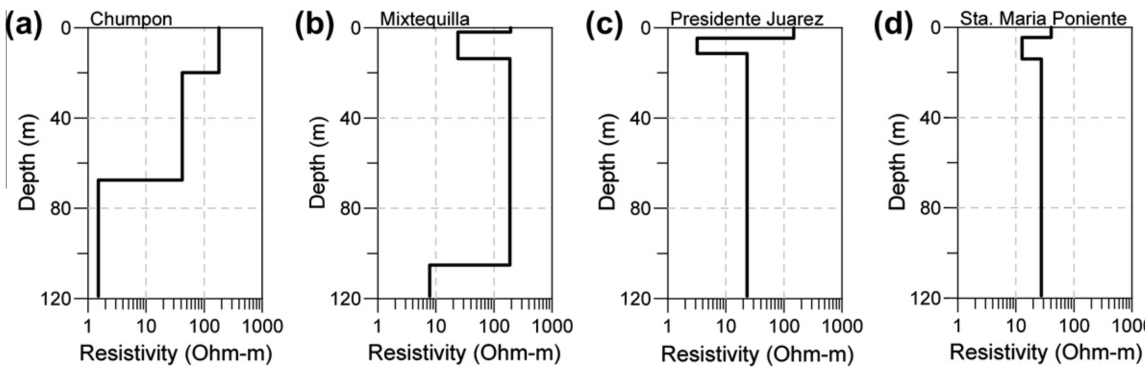

Fig. 5. Geological models inverted from TEM data. (a) shows the expected model, with only three layers, found in the flat area; (b)–(d) exemplify the locations where a shallow anomalous layer was found. Depth refers to depth below ground surface.

lens reached a thickness of 80–100 m 50–70 km from the coast. Ground truthing at site "Eden" (Fig. 1) showed good agreement. At Eden, Beddows (2004) found the halocline at 12 m below the water table during multiple measurements in wet and dry seasons. The TEM measurement yielded a depth to halocline of 16 ± 1 m below ground surface. Ground surface was 4–5 m above the water table.

The Dupuit–Ghyben–Herzberg model can be used to describe the position of the halocline in a homogeneous medium, if the interface is sharp, and the saltwater and freshwater bodies are in a steady state condition. The model describes the depth to the halocline, with respect to mean sea level, as a function of the elevation of the water table above mean sea level (Vacher, 1988):

$$z_i = 40 \cdot h_f \tag{9}$$

$$h_f = \sqrt{\frac{r}{41K}(L^2 - x^2)} \tag{10}$$

where z_i: depth to the halocline (mamsl), h_f: head of the freshwater lens (mamsl), K: homogeneous hydraulic conductivity (m/day), r: recharge (m/day), L: distance from water divide to coast (m), x: distance from water divide to point where halocline depth is calculated (m).

Water level observations were available within 2 km from the TEM sites. These water levels were plotted vs. depths to halocline (Fig. 4b). If the Dupuit–Ghyben–Herzberg relationship was valid, the points should be distributed along a line with slope −40 (Eq. (9)). Linear regression showed that the points followed a line with slope −39.2 (R^2 = 0.67). A statistical F-test showed that there is a significant relationship between the response (depth to halocline) and the regressor (water levels) (F-ratio: 32.86, p-value: 3×10^{-5}). A statistical individual t-test showed that the 95% confidence interval for the slope was [−47.8; −30.7] ($t_{16,0.975}$ = 2.120).

The Dupuit–Ghyben–Herzberg model (Eqs. (9) and (10)) was fitted to the data, using an estimated L = 100 km and $r = 5.5 \times 10^{-4}$ m/day (∼17% of mean annual precipitation). Although the Dupuit–Ghyben–Herzberg model is only valid for a homogeneous medium and steady state conditions, this was done to obtain a first order K-estimate of 0.3 m/s (Fig. 4a, root mean square error: 11.2 m).

3.2.2. A low-resistive shallow layer

The expected geology with a highly resistive top layer (unsaturated limestone, e.g. >100 Ωm), a medium-resistive middle layer (limestone saturated with freshwater, e.g. ∼50 Ωm) and a low-resistive bottom layer (limestone saturated with saltwater, e.g. ⩽5 Ωm) was observed in many TEM soundings (e.g. Fig. 5a). Some soundings were noisy in the first 285 Hz gates, and were therefore only trusted at depth. In contrast, seven sites revealed a lower-resistive layer (e.g. <20 Ωm) clearly present at shallow depth (e.g. Fig. 5b–d). The location of the sites is shown in Fig. 6b. The resistivity, depth and thickness of this layer at each site was not well determined using TEM. The method cannot accurately describe shallow layers, due to the time that passes from current turn-off till beginning of the first gate. Elevation of the top and bottom of the layer is shown in Fig. 6a – where error bars are not shown the depth is relatively undetermined from the inversion (infinite uncertainty).

3.3. Borehole logging results

The borehole logging results showed a difference in geology between the flat area and the hilly area/transition zone. In the five borehole logs carried out in the flat area, there were no significant anomalies. Two typical examples of flat area borehole logs are shown in Fig. 7a and b. These were the only two wells deep enough to penetrate the halocline (Fig. 7a) or the top of the saltwater/freshwater mixing zone (Fig. 7b), seen as an increase in the SEC fluid log and the induction log. The gamma logs did not have anomalies at the same depth as the induction-log anomalies, therefore the induction anomalies here are clearly due to saltwater entering the rock matrix.

Eleven borehole logs from the hilly area and transition zone showed some highly conductive layers with corresponding anomalies in the gamma logs. Examples of borehole logs with the anomalous layer are shown in Fig. 7c–e. The Supplementary material contains graphs of all eleven borehole logs containing the anomalous layer. Gamma-anomalies generally reached levels of about 80 counts pr. second (cps) and were located at the same depths as measured induction-log anomalies. Induction anomalies had values between approx. 200 and 800 mS/m (i.e. ∼5 Ωm down to ∼1.3 Ωm). The anomalies were generally 0–13 m below surface

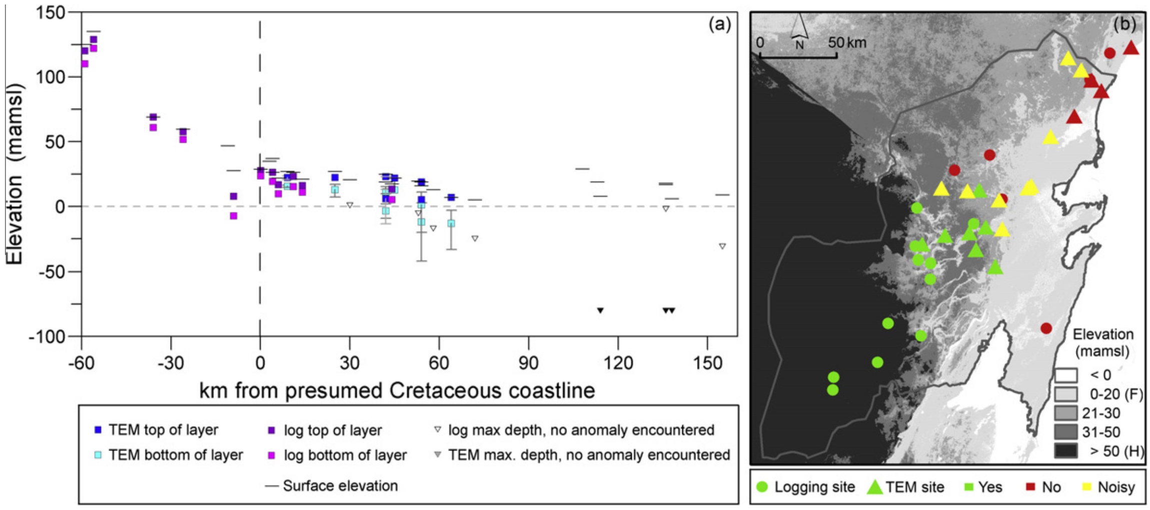

Fig. 6. (a) Elevation of the anomalous layer from TEM measurements and borehole logs. Surface elevation also shown, along with the max. measurement depth of the measurements which did not find the anomalous layer. Location of presumed Cretaceous coastline indicated, characterized by steep drop in elevation from 50 mamsl to <40 mamsl over less than 1 km; (b) location of TEM and logging measurements, with indications of which encountered the anomalous layer (green), which did not (red) and which were too noisy in the first gates to determine this (yellow). Background is SRTM topography, F = flat area, H = hilly area. (For interpretation of the references to color in this figure legend, the reader is referred to the web version of this article.)

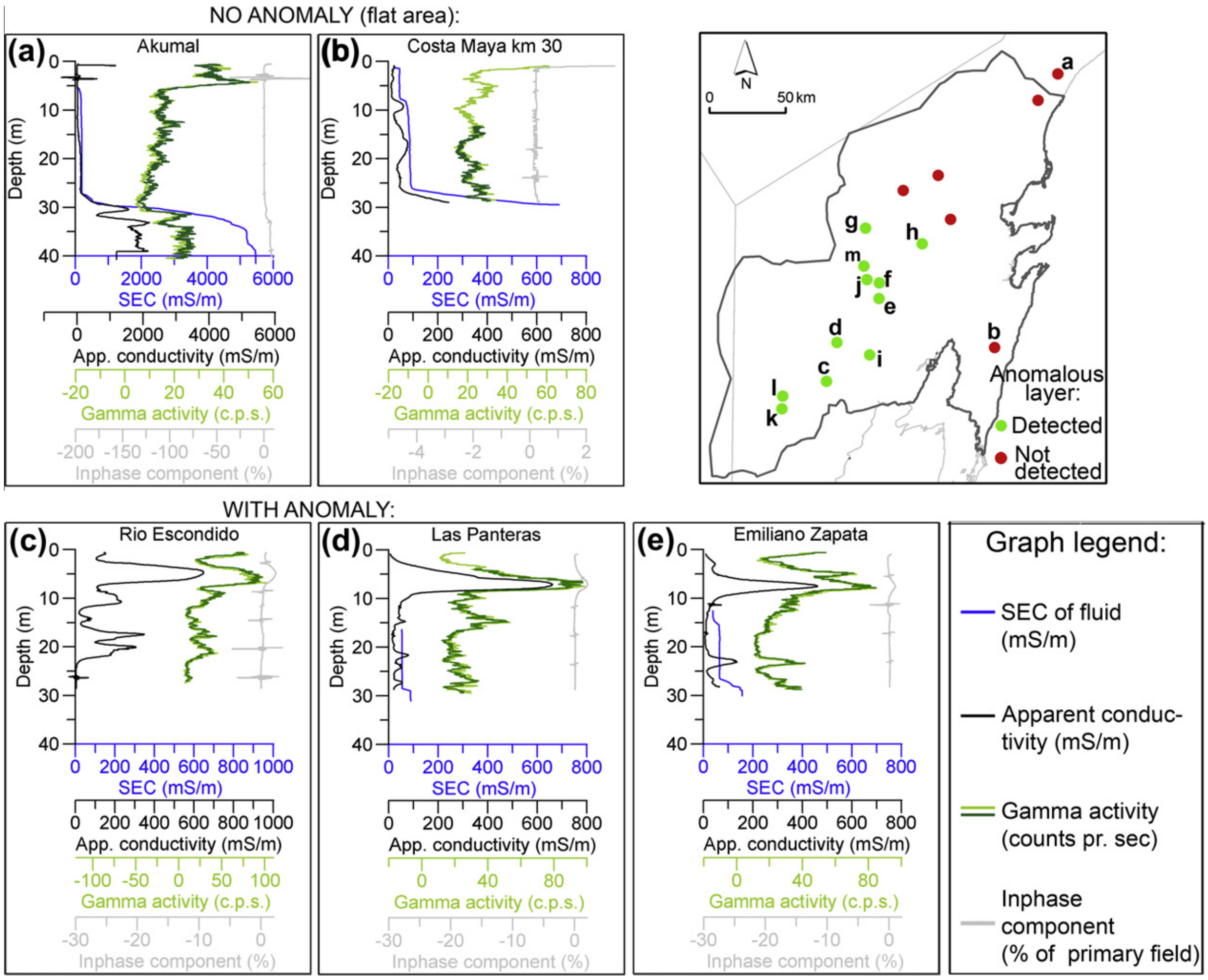

Fig. 7. Example results from the borehole logging. (a) and (b) represent typical results from the flat area (no anomalous layer detected). (c)–(e) show the logs with the anomalous layer detected. Results from remaining wells with anomalous layer given in Supplementary material. SEC: specific electrical conductivity of the well fluid – its top indicates location of water table. Location map at top right.

(mbs), 3–8 m thick, and located in the unsaturated zone. Elevation of the anomalies varied between sites (Fig. 6a). The Reforma site was an exception, with the anomaly located in the upper part of the aquifer, at 20–35 mbs.

One well, Xpichil, was located in the transition zone but did not encounter the anomalous layer. This well was only logged down to 20 mbs (down to 0.82 mamsl).

Metal clamps on most PVC well casings were responsible for the regularly spaced thin positive and negative anomalies seen in the induction log and the inphase component. The inphase thus indicated which anomalies were due to geology and which were due to well casing features.

3.4. Geochemical results

Full water chemical results and saturation indices calculated with PHREEQC are given in the Supplementary material. Here only the most relevant results are described. An electrical balance between 1.0 and 7.5 meq/L (1.0–12.7%) showed that no major elements were missing from the chemical analysis.

The ratio 1000·Sr/Cl (Fig. 8a) indicates the degree of influence of modern day sea water. Modern day seawater at Yucatan has a 1000·Sr/Cl-ratio of 0.11 (Stoessell et al., no year). If this ratio is >10 there is little or no mixing with modern day sea water. Fourteen of the 31 sampling points fell within this category. These points were mainly located in the Cretaceous geology. The remaining seventeen samples had 1000·Sr/Cl-ratio between 1 and 10. This category mainly encompassed water from the Pliocene area, but some sites in the Cretaceous area also had values between 1 and 10.

Samples with Cl/Na-ratios between 1 and 1.17 indicates that the source of Cl is seawater dilution or halite dissolution. This was only the case for six samples: Andres Quintana Roo, Limones, Pedro A. Santos and Polinkin in the Pliocene area, and Nicholas Bravo and Veinte de Noviembre in the Cretaceous area. No value of the Cl/Na ratio occurred distinctly more often than the others (Fig. 8b), and most Cl/Na-ratios were below the halite or seawater values.

All water samples had a relatively high content of the strontium-ion. The Sr-content was much larger than it would be if seawater was the sole contributor of this ion to the water (Fig. 9a and b), and there was no correlation between Sr and Cl contents (Fig. 9b). An excellent linear correlation however existed between the concentration of the Sr and the SO_4 ions (R^2 = 0.95, Fig. 9a). The Sr-concentrations were higher than the seawater value of 0.16 meq/L (Stoessell et al., no year) for 10 of the 31 samples; all of these were located in the Cretaceous geology.

The 100·SO_4/Cl-ratios were grouped into three categories (Fig. 10a): Ratios >100, ratios between 10 and 100 and ratios below 10. The ratios >100 were found in the Cretaceous area and the transition zone part of the Pliocene area. The ratios between 10 and

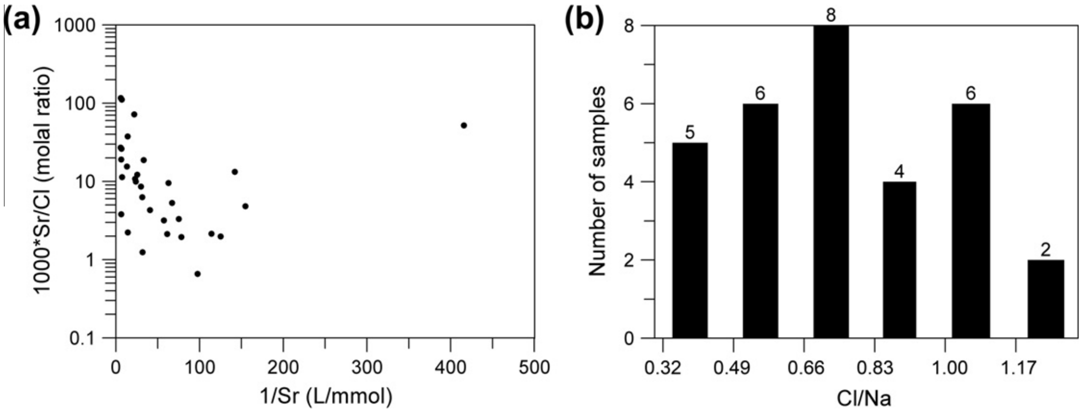

Fig. 8. (a) Molal ratio of 1000·Sr/Cl vs. 1/Sr in L/mmol. (b) Histogram of Cl/Na ratio (in equivalents). If the water obtained its Cl from saltwater or halite, this ratio would be between 1 and 1.17, a criteria only fulfilled by six samples.

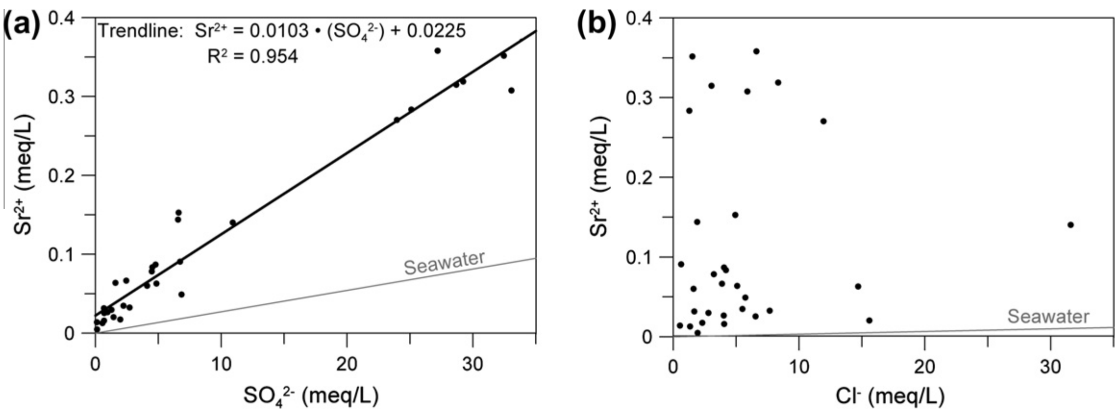

Fig. 9. (a) Sr-concentration vs. SO_4-concentration, along with linear fit (bold black line and equation given) and the distribution for seawater (grey line). (b) Sr-concentration vs. Cl-concentration, along with the distribution typical for seawater (grey line).

100 were found in the flat area and in a belt at the southern part of the hilly region (Fig. 10a). In the same places where this ratio was >100, high absolute concentrations of the sulfate ion were found (Fig. 10c) and these waters were very close to or at saturation with gypsum, celestite and anhydrite (Figs. 10b and 11b–d). Furthermore, a strong linear correlation was seen between the dominant cations Ca and Mg and the sulfate concentration (R^2 = 0.98, Fig. 11a).

3.5. ET and recharge results

The estimated daily ET_a for the whole Peninsula (spatial average) was rather stable from year to year, and varied temporally from 1.56 to 3.90 mm/day (mean: 2.63 ± 0.51 mm/day) (Fig. 12a). Lowest values were encountered in the late wet season (November–January) whereas highest values occurred in the late dry and early wet season (March–August). The correspondence with ET_{ref} shows that the net radiation is the main determining factor for the temporal variation (Fig. 12a). On a spatial average, ET_a exceeded average monthly precipitation during November–April (Fig. 12a). Spatially, the temporal average ET_a for 2004–2008 varied between 0.99 and 6.93 mm/day (mean: 2.62 ± 0.52 mm/day) throughout the Peninsula. When considering only the study area, ET_a varied between 1.42 and 5.74 mm/day (mean: 2.88 ± 0.42 mm/day). The highest ET_a-rates were seen at the coast, where elevations <10 mamsl, and hence water table was relatively close to ground surface. Lowest rates were seen in the drier and less densely vegetated Yucatan State.

Recharge was estimated according to Eq. (1) by subtracting estimated ET_a from precipitation. A comparison of the two quantities for 2004–2008 showed that mean annual ET_a constituted 70–89% of mean annual precipitation on a Peninsula average (Fig. 13a). The variation was chiefly due to yearly variation in precipitation amounts. On average, recharge on the Yucatan Peninsula was thus estimated to be 23% of mean annual precipitation. When considering only the study area, the average value was 17%, when considering an ET_a average of years 2004–2008 and average precipitation covering the same time period. Spatial distribution of recharge showed that ET_a exceeded mean annual rainfall along the coasts (Fig. 13b). In the study area, main recharge areas were located in the hilly area and the area towards Valladolid. Yearly average recharge for the whole Peninsula was 0.79 ± 0.70 mm/day (max.: 3.16 mm/day, min.: −4.01 mm/day); average recharge for the study area was 0.56 ± 0.55 mm/day (max.: 2.24 mm/day, min. −2.49 mm/day).

4. Discussion

4.1. Hydrogeological differences across the study area

The observed regional difference in water levels and hydraulic gradients indicates a difference in transmissivity across the study area. The low hydraulic gradient of the Pliocene area (3–7 cm/km) corresponds well with hydraulic gradients measured elsewhere in the Yucatan Peninsula (Yucatan State: 2 cm/km (Back and Hanshaw, 1970), 0.7–1 cm/km (Marín, 1990); Riviera Maya:

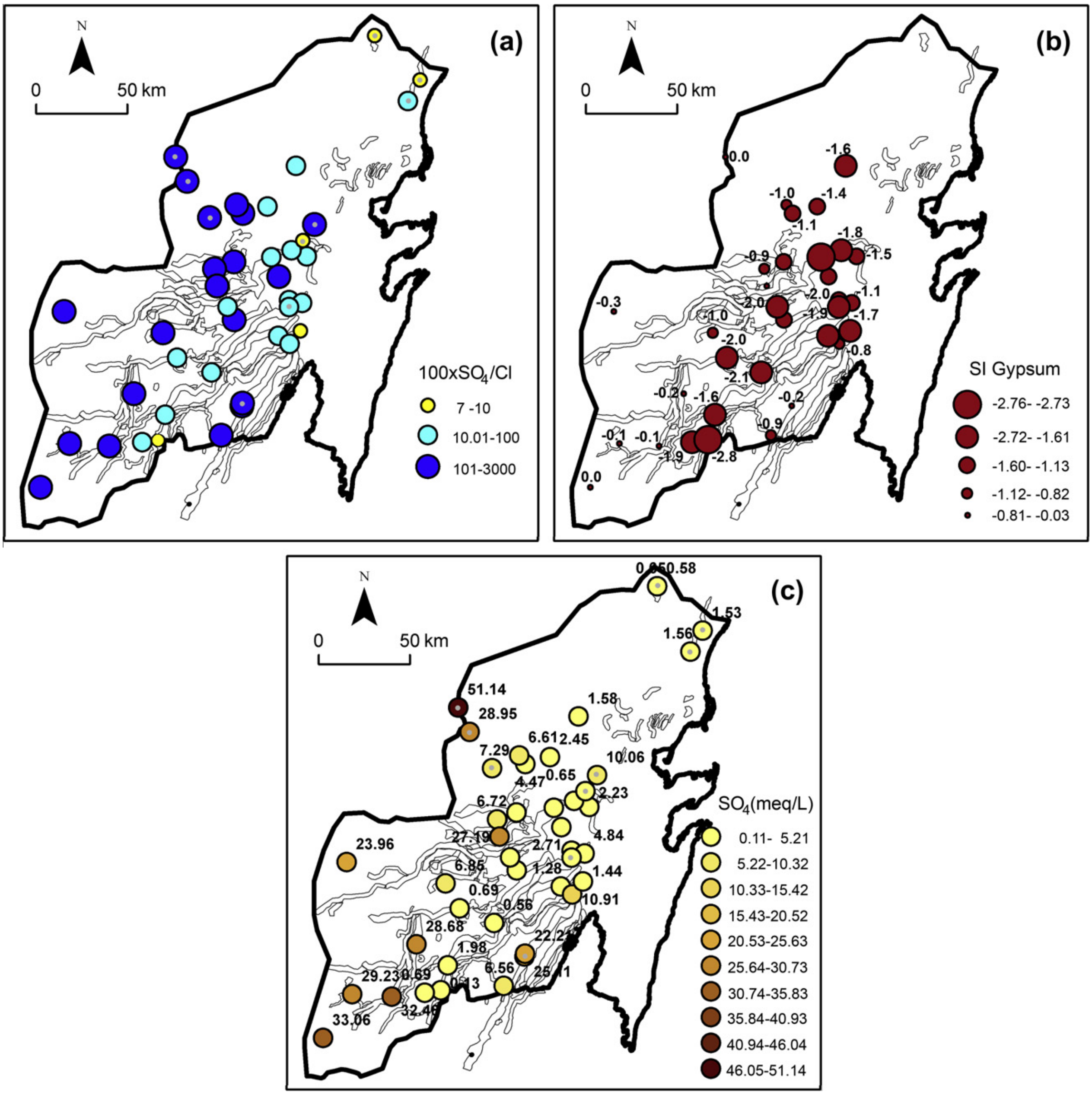

Fig. 10. Spatial distribution within the study area of (a) 100 · SO_4/Cl-ratios (in equivalents), (b) gypsum saturation indices, and (c) SO_4-concentrations (meq/L). The 10 small grey dots indicate results from Perry et al. (2002) (mainly) and Stoessell et al. (no year) (only Chumkopo site).

10–15 cm/km (Moore et al., 1992), 6 cm/km (Beddows, 2004)). The water level variations have the same magnitude as those reported for Yucatan State (5–61 cm within 2.5 years, Marín, 1990). These low values indicate high transmissivity of the geology in the Pliocene area. The small and smooth variations in hydrographs from the Pliocene areas support a high transmissivity here. The relatively large $K = 0.3$ m/s estimated from data and Eq. (10) has the same order of magnitude as that calculated from field data by Moore et al. (1992) and that used in hydrological modelling by González-Herrera et al. (2002).

In the Cretaceous geology the transmissivity may be much lower. Low transmissivity could explain the much higher hydraulic gradient and the large spatial variation in the believed regional water table, e.g. at La Lucha (91.7 mamsl) and Nuevo Becar (34.7 mamsl), located only 30 km apart (Fig. 2b and c). Another option could be that all water in the Cretaceous geology is perched. This however still indicates low transmissivity of the Cretaceous geology or of beds herein.

A geological difference between the two areas is supported by geochemistry. The Cretaceous geology appears to contain significant amounts of evaporites, e.g. gypsum and anhydrite. Firstly, this is seen from the clear correlation between Ca^{2+} and SO_4^{2-} (Fig. 11a). Gypsum dissolution would give such a clear correlation, and in all points the 100·SO_4/Cl-ratio were higher than that of seawater (=10.3, Perry et al. (2002)), indicating some up-concentration compared to the marine environment. Secondly, sampling points located in the Cretaceous geology were close to saturation with gypsum and anhydrite (Figs. 10b and 11b and d). Thirdly, the spatial distribution of the highest 100·SO_4/Cl-ratios (>100) indicates the region affected by evaporites (Fig. 10a) (Perry et al., 2002). The spatial distribution of these geochemical indications of evaporites corresponds very well with the location of the Cretaceous

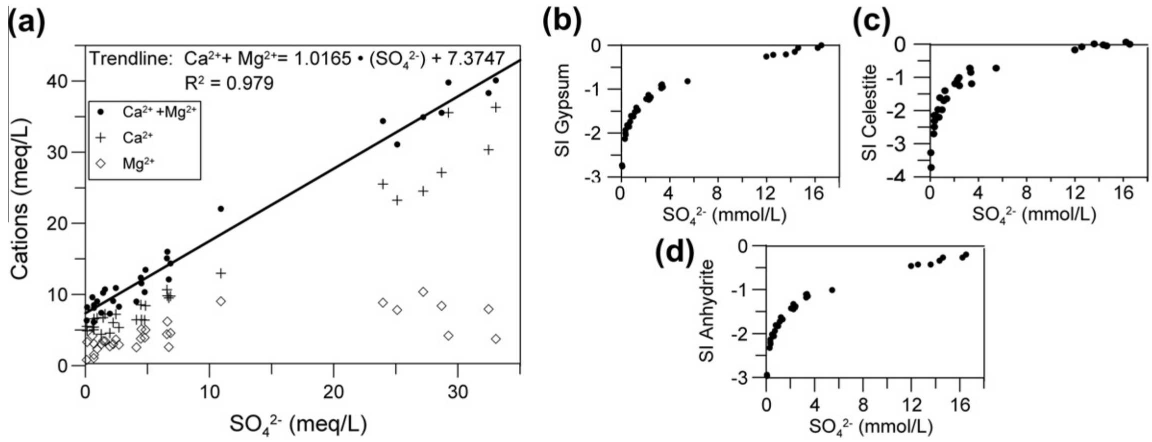

Fig. 11. (a) Ca, Mg and (Ca + Mg) concentrations vs. SO_4-concentrations (meq/L), (b)–(d) gypsum, celestite and anhydrite saturation indices (no unit) vs. SO_4-concentrations (mmol/L).

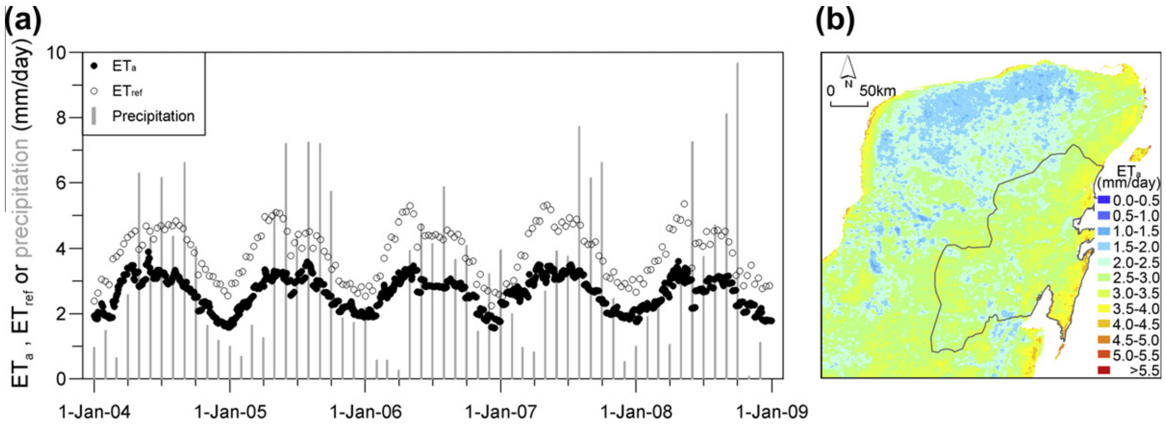

Fig. 12. (a) ET_a temporal daily variation; (b) ET_a spatial variation (average of years 2004–2008). (a) Also includes ET_{ref} estimated using Hargreave's equation, and monthly average precipitation from TRMM.

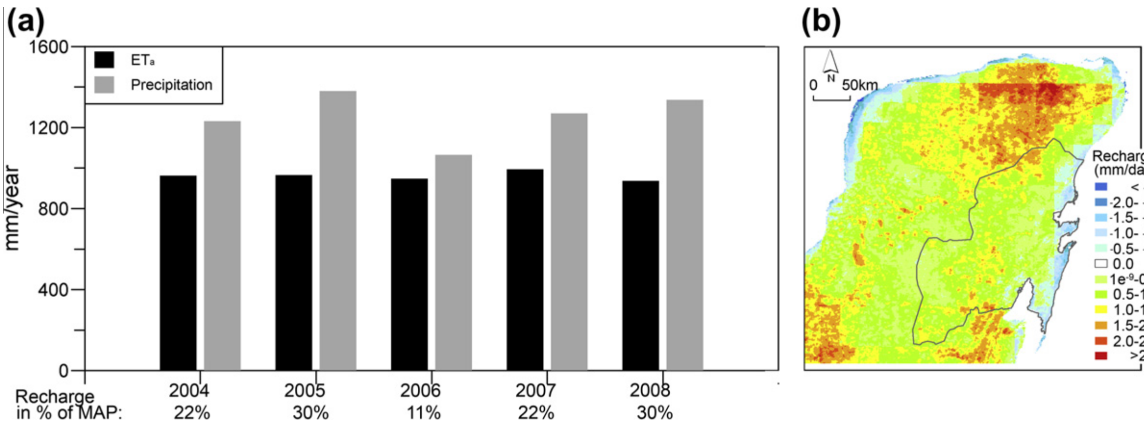

Fig. 13. Recharge, calculated as mean annual precipitation subtracted ET_a (both average of 2004–2008); (a) temporal variation, displayed together with average Peninsula precipitation from TRMM and calculated ET_a, (b) spatial variation (mm/day).

geology (Fig. 1), and the gypsum quarries shown in Perry et al. (2009). Likely this area may belong to the evaporitic Ichaiche formation (e.g. Lopez-Ramos, 1975). Schönian et al. (2005) described that the Ichaiche formation is probably Cretaceous of age, instead of the Paleocene age which has been proposed for it, and his boundary to the Ichaiche formation corresponds well with the boundary between Cretaceous and Miocene sediments in Fig. 1. Deep drilled wells in Yucatan State have also encountered Cretaceous sediments with gypsum, anhydrite and halite (Lefticariu et al., 2006; Rebolledo-Vieyra et al., 2000). The belt with lower 100·SO_4/Cl-ratios corresponds with the location of Miocene sediments. This area also has generally low gypsum saturation indices and SO_4^{2-}-concentrations. Two sites in this Miocene geology stand out by having the same water-chemical signature as the Cretaceous sediments

(Fig. 10a–c). This may be due to inadequate placement of geological boundaries, so that the points are in fact located in Cretaceous geology. Another explanation may be that these sites are influenced by water from deeper geological layers, as they are located close to the fault that forms Laguna de Bacalar, mapped as up to 15 m deep and associated with four surrounding cenotes >90 m deep (Gischler et al., 2008). The southern end of the fault (outside the study area) extends close to the Cretaceous boundary, making transport of water affected by Cretaceous sediments through the fault another possibility. Gypsum is known to have low primary porosity, with water flow mainly taking place through developed karst features, if any (Klimchouk, 1997). Cretaceous anhydrite samples from a borehole in Yucatan State generally have a porosity <2% (Mayr et al., 2008). This supports the proposed lower transmissivity suggested by the water level data. Perry et al. (2002) defined the 'Evaporite Region' as extending south and east of Lake Chichankanab "from somewhere between Tulum and Felipe Carrillo Puerto south to the Belize border". Due to denser sampling this study can now define the region influenced by evaporites more precisely. The $100 \cdot SO_4^{2-}/Cl$ – ratios og $SO)_4^{2-}$ concentrations are in agreement with those found by Perry et al. (2002, 2009) (also plotted in Fig. 10 for completeness).

The measured high sulfate concentrations likely originate from gypsum dissolution, since their locations correspond to the gypsum-associated areas mentioned above. The geological control on water quality is important to realize for the water management authorities, because high sulfate concentrations (e.g. concentrations >9.4 meq/L, Marfia et al., 2004) may impair water quality. Twelve samples exceeded 6 meq SO_4^{2-}/L, seven of which had concentrations >20 meq/L. These sites coincided with places in the Cretaceous geology where local residents complained about bad taste of the water.

The geochemical results also indicate some heterogeneity. For instance large differences in water chemistry were seen between Presidente Juarez and Nuevo Israel, located only 9 km apart. A similar example has been reported in Chunhuhub (Perry et al., 2009), and local-scale heterogeneity was also indicated in the geological mapping of Kenkmann and Schönian (2006). Limited hydraulic permeability may explain such water quality heterogeneity, as also suggested by Perry et al. (2009). Alternatively, geochemical heterogeneity may be caused by rapid water flow through preferential flow paths (caves, faults), enabling water from different geochemical regions to be transported to other regions without equilibrating with the surrounding matrix.

A last regional difference in hydrogeology is the suggested presence of perched aquifers mainly found in the Cretaceous geology or close to its boundaries. To our knowledge, this is the first time that perched aquifers in the region have been mapped (Fig. 2a). Other authors (Perry et al., 2009; Pope and Dahlin, 1989) have only in general terms mentioned presence of perched water tables. The large temporal water level changes in the perched aquifers are caused by direct recharge by local precipitation and likely also by (seasonal) surface water runoff. A barrier of low permeability reducing infiltration rates from the perched aquifer to deeper geological layers must necessarily exist in this area. Likely different types of recharge and storage pertain to the perched aquifers and the regional aquifer in the Pliocene area. The jagged hydrograph (Fig. 3a) indicates concentrated recharge and/or low storage and/or concentrated flow (Kiraly, 2003). The smooth hydrographs (Fig. 3b and c) indicate the opposite.

4.2. Areas influenced by saltwater intrusion

In the Pliocene area the TEM measurements clearly detected saltwater underlying the freshwater. Together with the distribution of the 1000·Sr/Cl-ratios <10 the TEM data support that the Pliocene area is influenced by saltwater intrusion. Since the Dupuit–Ghyben–Herzberg slope of −40 falls within the 95% confidence interval of the slope calculated from the data, the Dupuit–Ghyben–Herzberg model is valid for the sampled area when taking a large-scale perspective. The freshwater can therefore be conceptualized as a lens, and Eq. (9) may be used to define the lower level of the freshwater aquifer in the Pliocene area, based on measured and modelled water levels. In Yucatan State Eqs. (9) and (10) were also found valid at a regional scale (Steinich and Marín, 1996). On a local scale the model may not be valid because the basic assumptions of the model are not fulfilled. Geological heterogeneity, non-stationary conditions etc. may account for the fluctuation of points around the Dupuit–Ghyben–Herzberg model curve. On a local scale, neither Moore et al. (1992) nor Beddows (2004) found Eqs. (9) and (10) to fit their measured depths to halocline. Both studies were conducted on a local scale and relatively close to the coast (max. 20 km inland, most sampling undertaken within 10 km of the coast). On a local scale coastal caves may truncate the depths to the halocline (Wicks and Herman, 1995), and an outflow face (Van der Veer, 1977; Vacher, 1988), affecting Eq. (10), may need to be applied as a boundary at the coast (Beddows, 2004).

In the Cretaceous geology there is no evidence for the presence of saltwater beneath the freshwater in the regional aquifer. The 1000·Sr/Cl-ratios are generally >10 here, indicating little influence by modern day seawater. At the same time most Cl/Na-ratios in this area do not indicate influence of seawater dilution. Perry et al. (2002) found Cenote Azul, located in the Miocene geology, to have an unusually low chloride-content (1.2 meq/L). This study shows that a low chloride-content is not unusual in the areas with surface geology older than Pliocene. Eight sites had Cl-concentrations <2 meq/L (see Supplementary material). In Cenote Azul, scuba divers have so far found 74 m of freshwater column, and have not encountered any saltwater despite the proximity to the coast (P. Widmann, freelance cave diver, personal communication, 2008). Two possibilities exist. Either the saltwater is very deep down in the older geology (water table elevations and Eq. (9) would indicate a halocline 400–3600 m below mean sea level; whether such a thick water column is realistic could be disputed) or there is no saltwater intrusion in this region. Whichever the possibility, it remains that the older geology does not appear affected by saltwater intrusion. Perry et al. (2009) came to the same conclusion, but defined the unaffected area as being "along the southernmost Caribbean coast from somewhere south of Tulum to the Belize border and probably much farther south". This study has mapped the unaffected and affected areas more precisely.

Six sites had Cl/Na-ratios that indicated the source of chloride to be either seawater dilution or halite dissolution. Four of the sites were in the Pliocene area, favoring the former explanation. The remaining two sites were located in the Cretaceous and Miocene areas. Possibly local halite deposits may explain their data.

4.3. The low-permeable shallow geological layer – interpretation and hydrogeological effect

The similar magnitude of the borehole log anomalies at the 11 different sites, and their generally similar depths indicate that these anomalous layers likely represent the same stratigraphic unit. Furthermore, the gamma anomaly (90 cps) at 1–4 mbs in the Presidente Juarez borehole log is at the same depth interval as a highly conductive layer found using TEM at a different site in the same village (~313 mS/m = 3.2 Ωm, top of layer located 3.4–6.2 m below surface (=one standard deviation interval), Fig. 5c). The depths and thicknesses of the low-conductive layers detected with TEM are in the same range as those detected in the borehole logs (Fig. 6a). The low-conductive layer detected with TEM is thus likely to be the same stratigraphic unit as the anomalous layer found in the borehole logs.

The low resistivity and high natural gamma activity of the layer indicates that the layer is possibly a fine-grained, clayey material. It has not previously featured in geological maps of the area. One possibility is that this layer is ejecta from the Chicxulub impact at the Cretaceous/Paleogene boundary. The apparent properties of the layer correspond with ejecta properties in general. The ejecta is reported to consist of larger clasts deposited in a fine-grained matrix (Ocampo et al., 1996; Pope et al., 2005). Clayey and silty material characteristically exhibit high natural gamma-radiation. The ejecta layer is characterized by high conductivity and gamma anomalies in other borehole logs (Grajales-Nishimura et al., 2000; Wohlgemuth et al., 2004; Mayr et al., 2008). Furthermore, one ejecta location mapped by Schönian et al. (2004, 2005) is 2 km from one of the logged wells where the anomalous layer was found (Reforma).

Additionally, the geochemistry indicates the possible presence of ejecta. The lack of correlation between Sr and Cl, and the excellent correlation between Sr and SO_4 ions indicates that the Sr-content likely originates from dissolution of celestite present in evaporite and/or in ejecta (Perry et al., 2002, 2009). Perry et al. (2002) found the same correlation for their groundwater samples taken south and west of Lake Chichankanab. Especially where Sr-concentrations are higher than seawater's, water may be in contact with evaporite or ejecta layers (Perry et al., 2009). This was the case for ten samples. Application of the following formula (Perry et al., 2009):

$$m_{SrE} = m_{SrGwtr} - (Cl_{Gwtr}/Cl_{Sea}) \cdot m_{SrSea} \quad (11)$$

where m_{SrE}: mmol evaporite Sr pr. L of sample; m_{SrGwtr}: Sr-concentration in sample (mmol/L); (Cl_{Gwtr}/Cl_{Sea}): ratio of Cl-concentration in sample to that in seawater (–); m_{SrSea}: Sr-concentration in seawater (mmol/L) reveals that the amount of "excess" strontium (m_{SrE}) contributed to a water sample by dissolution of evaporite was $\geqslant$0.05 mmol/L at ten sites; in seven cases even as large as 0.13–0.18 mmol/L. All these sites were again located in the hilly area and transition zone, mainly in the Cretaceous geology. Of these, the sites in the hilly area were close to saturation with celestite, gypsum and anhydrite.

A way to prove presence of Chicxulub ejecta in the anomalous layers is by microscopy of thin sections, e.g. to confirm presence of shocked quartz, altered glass and "peening texture" (Ocampo et al., 1996; Pope et al., 2005; Schönian et al., 2004; Marshall et al., 1998). This has not been possible within this study. Nevertheless, whether the anomalous layer in borehole logs and TEM specifically represents the ejecta layer or merely "a clay layer", the results indicate that this layer is widespread in the hilly region and the transition zone. Airborne frequency-domain electromagnetic measurements (HEM) over five transects in the hilly area and transition zone also indicate the presence of the high-conductive layer throughout these areas. The HEM data were modelled well with an anomalous layer of the same thickness, depth and resistivity as seen in nearby borehole logs (Gondwe et al., submitted for publication).

The ejecta was deposited atop a karstified Cretaceous surface (Pope et al., 2005). Possibly only the present hilly area was land surface, permitting weathering and karstification to create greater variation in the topographic relief here compared to surrounding areas. The surrounding water-covered areas would have had a more modest relief. Assuming that the anomalous layer is ejecta, these circumstances may explain why the anomalous layer is found at widely varying elevations in the hilly area, but at similar elevations in the transition zone (Fig. 6a and results in Gondwe et al., submitted for publication). Between the hilly area and the transition zone there is today a steep drop in elevation of more than 10 m (from 50 to <40 mamsl) within less than 1 km suggesting the presence of an ancient coastline here, and distinguishing the two areas of notably different topographic relief.

If the anomalous layer is ejecta, erosion may have taken place following the deposition, reducing the thicknesses of the layer from the 200–400 m thick deposits found in wells near the impact crater (Rebolledo-Vieyra et al., 2000; Urrutia-Fucugauchi et al., 1996, 2004, 2008) to the 3–8 m seen in most borehole logs. A weathered ejecta surface beneath Cenozoic sediments has been found (Pope et al., 2005) and Urrutia-Fucugauchi et al. (2008) also suggested significant erosion of the ejecta blanket after finding a ~34 m thick ejecta unit beneath Cenozoic sediments near Valladolid. Other ejecta findings away from the crater have reduced thicknesses too (Pope et al. (2005): 4–8 m, bases not always observed; Ocampo et al. (1996): 16 m). After erosion, the transition zone and the most southern part of the hilly area near the Bay of Chetumal would have been covered by Cenozoic sediments, according to the geologic map (Fig. 1).

In the flat area no anomalous layer has been found at the depths explored in this study, and the geochemical results do not indicate interaction with ejecta/evaporite. Likely the layer is buried deeper here. Furthermore, the freshwater lens is thinner in this near-coastal zone, reducing the likelihood of freshwater interacting with ejecta layers. The ejecta layer has in Yucatan State been encountered at 222, 250, 257, 332 and 795 mbs, corresponding to about −190 to −780 mamsl (Urrutia-Fucugauchi et al., 2008; Rebolledo-Vieyra et al., 2000; Lefticariu et al., 2006).

Whether or not the anomalous layer is ejecta, a hydrogeological implication of the documented shallow and likely clayey (i.e. low-permeable) layer may be the formation of perched aquifers and ephemeral swamps and streams seen in the transition zone and hilly area. The anomalous layer appears widespread, and may be continuous. However karstic features such as cenotes may interrupt the layer and locally erosion may have removed the layer completely. The layer likely does not generally inhibit infiltration on a regional scale. Locally, it may however reduce infiltration. Examples are the formation of the ephemeral surface water bodies, and the flooding of villages and roads, which occurs in and near the hilly area during the rainy season and lasts for several weeks to months after rainfall events. A recent study by Perry et al. (2010) has similarly found evidence of an extensive clay-rich aquitard in neighboring Campeche.

4.4. Conceptual hydrogeological model

The hydrogeological results are summarized in the conceptual model presented in Fig. 14. If the anomalous shallow geologic layer is interpreted as ejecta, the underlying material must necessarily be of Cretaceous age. As the transition zone has a high hydraulic permeability, the rather shallow Cretaceous material here is likely not evaporitic, but rather karstified limestone and/or dolomite, for instance the Barton Creek formation or the Cerro de Pavo formation (Pope et al., 2005; Schönian et al., 2005; Butterlin, 1958). In contrast, the Cretaceous formation in the hilly area appears to generally have a low matrix permeability and evaporitic geochemical signature, and could for instance be the evaporitic Ichaiche formation (Schönian et al., 2005; Lopez-Ramos, 1975). If the anomalous geologic layer is not ejecta, the Cenozoic sediments (likely the Carrillo Puerto formation, e.g. Butterlin, 1958; Lopez-Ramos, 1975) could solely account for the high permeability of the transition zone and flat area throughout the depth of the freshwater lens. No boreholes have yet documented the thickness of the Cenozoic sediments in the study area, so both scenarios are plausible.

Saltwater intrusion is documented in the flat area and transition zone, but is unknown in the hilly area. Fresh groundwater flow takes place in both rock matrix and preferential flow paths, such as caves. Large-scale structures and faults, discernable from remote

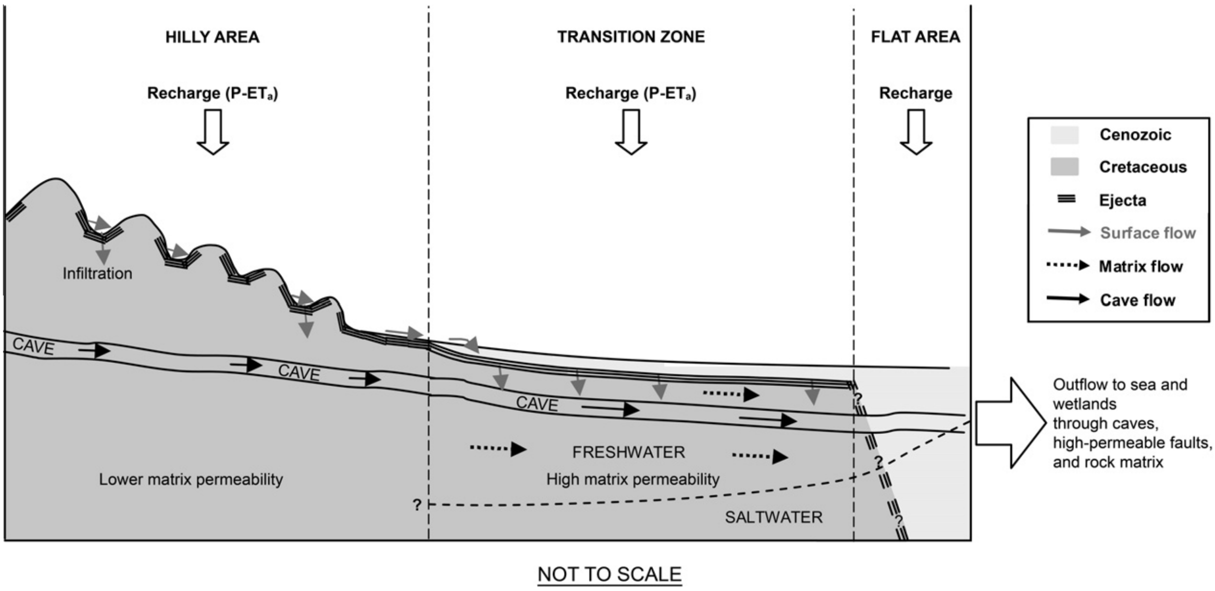

Fig. 14. Conceptual model with the anomalous layer interpreted as ejecta.

sensing imagery, is present throughout the hilly area and transition zone, and may represent large-scale preferential flow paths within the study area (Gondwe et al., submitted for publication, 2010). Ephemeral surface water flow takes place in the hilly region and in part of the transition zone, mainly atop the large-scale structures. The surface water eventually infiltrates to the groundwater, through the unsaturated zone and through sinkholes, except the little surface water which connects to Río Hondo and flows out into the Bay of Chetumal. The overall groundwater levels and the presence of the structures indicate the possibility of significant above- and underground transfer of groundwater from the hilly area to the transition zone.

The spatial distribution of recharge is dominated by vegetation patterns. The high recharge areas in the hilly area and towards Valladolid are characterized by less dense or smaller vegetation, reflected in relatively lower EVI. In the hilly area, most of the high-recharge locations correspond to the structures outlined in Gondwe et al. (submitted for publication), owing to the generally smaller vegetation of the swampy areas (Tun-Dzul et al., 2008). Near the coast average evapotranspiration rates exceed average precipitation rates. That is possible due to flow of groundwater from the inland areas to the coast. The comparatively higher evapotranspiration rates at the coast may be related to the water table being closer to the ground surface in these areas, yielding a thinner unsaturated zone. Possibly, the groundwater becomes accessible to plant roots in these areas, providing an unlimited source for evapotranspiration. A spatial view of evapotranspiration has not previously been presented for the Yucatan Peninsula.

Average recharge is relatively high, but agrees well with previous estimates. Lesser (1976) calculated ET_a to be 900 mm/year using Turc's method for the northern half of the Yucatan Peninsula, meaning that recharge would constitute 15% of the average rainfall in his area of study. This study found average ET_a for the whole Peninsula to be between 937 and 995 mm/year. Thomas (1999) estimated recharge to be 21% and 23% of mean annual precipitation for Chetumal and Valladolid. This is in the same range as the average annual values calculated in this paper for the study area and for the whole Peninsula. Beddows (2004) suggested that recharge should be >30% of mean annual precipitation at the coast to match field data of outflow from two cave systems, and to match halocline depths in an area <10 km from the coast. In contrast, this study suggests limited average recharge rates at the coast. Flow of groundwater from distant parts of the catchment to the coast might instead explain Beddows' data.

5. Conclusions

Water level data and geochemistry show that there is a distinct hydrogeologic divide within the study area, related to a topographic divide and a change in the age of sediments exposed at the ground surface. The hilly area, with Cretaceous sediments, has a lower hydraulic permeability, whereas the transition zone and flat area, which includes younger sediments, has a high permeability. The transition zone and flat area is influenced by saline intrusion, and the freshwater can here be conceptualized as a Dupuit–Ghyben–Herzberg lens. In the hilly area evidence of saline intrusion has not been found.

A shallow low-resistive layer is present in the hilly area and the transition zone, evidenced from geophysical measurements. The layer also has high natural gamma activity. This is the first time this layer is documented throughout the region. The layer is proposed to be continuous or nearly continuous in the region. It is suggested that the layer may be ejecta from the Cretaceous/Paleogene Chicxulub meteorite impact. The dataset thus represents an input to the ongoing discussion on the distribution of the ejecta blanket. Two different conceptual hydrogeological models are proposed, depending on whether the layer is ejecta or rather an unspecified clayey layer, previously unmapped in the region (Fig. 14). The anomalous layer is likely responsible for the formation of local perched aquifers and ephemeral surface water bodies in the region.

The developed conceptual model contributes with new hydrogeological knowledge of the region, and is an important prerequisite for hydrological modelling and sound groundwater management within the study area. The multidisciplinary methodology applied is applicable for other catchment-scale studies in karst and unmonitored regions.

Acknowledgements

We gratefully acknowledge financial support from the WWF Verdensnaturfonden/Aase and Ejnar Danielsens Fond 2006 and 2007, the COWI foundation, and the Technical University of

Denmark. This study would not have been possible without field support (equipment and/or field assistants) from Amigos de Sian Ka'an, UNAM, CICY-CEA, the Geological Survey of Austria and ETH Zürich. We thank CONAGUA for climate data, access to CONAGUA boreholes and for a list of licensed private boreholes in Quintana Roo, which strongly helped us locate useful boreholes for logging. We thank CAPA for access to log the Carrillo Puerto well and for water chemical data from municipal water wells. We thank well operators and private ranch owners for granting us access to sample water from and log in their wells. Oxygen isotope analyses of water samples (results shown in the Supplementary material) were kindly performed at Centre for Ice and Climate, Niels Bohr Institute, University of Copenhagen, Denmark. We are thankful for the thorough comments from two anonymous reviewers, which greatly improved this manuscript.

Appendix A. Supplementary material

Supplementary data associated with this article can be found, in the online version, at doi:10.1016/j.jhydrol.2010.04.044.

References

Allen, R.G., Pereira, L.S., Raes, D., Smith, M., 1998. Crop evapotranspiration. Guidelines for computing crop water requirements. FAO irrigation and drainage paper, 56. Rome, FAO. ISBN 92-5-104219-5.

Anderson, M.C., Norman, J.M., Diak, G.R., Kustas, W.P., Mecikalski, J.R., 1997. A two-source time-integrated model for estimating surface fluxes using thermal infrared remote sensing. Rem. Sens. Environ. 60, 195–216.

APHA, 1998a. Method 2320-B. Alkalinity. Titration Method. Standard Methods for the Examination of Water and Wastewater, 20th ed. American Public Health Association. Washington, DC, pp. 2–27.

APHA, 1998b. Method 2320-B. Sulfate. Turbidimetric Method. Standard Methods for the Examination of Water and Wastewater, 20th ed. American Public Health Association. Washington, DC, pp. 4–1888.

ASK, 2003. Tratamiento de Aguas Residuales. Report prepared by Amigos de Sian Ka'an A.C. (ASK). Available on the cd-rom of the workshop: Construyendo las Bases Para la Conservación del Agua y su Biodiversidad Asociada en la Península de Yucatan". 10 y 11 de noviembre 2003, Cancún Quintana Roo, Organizado por Amigos de Sian Ka'an, The Nature Conservancy y la Comisión de Áreas Naturales Protegidas.

Back, W., Hanshaw, B.B., 1970. Comparison of chemical hydrogeology of the carbonate peninsulas of Florida and Yucatan. J. Hydrol. 10, 330–368.

Beach, T., Luzzadder-Beach, S., Dunning, N., Cook, D., 2008. Human and natural impacts on fluvial and karst depressions of the Maya Lowlands. Geomorphology 101, 308–331. doi:10.1016/j.geomorph.2008.05.019.

Beddows, P.A., 2004. Groundwater hydrology of a coastal conduit carbonate aquifer: Caribbean coast of the Yucatán Peninsula, México. PhD thesis, Sch. of Geogr. Sci. Univ. of Bristol, UK.

Beddows, P.A., Smart, P.L., Whitaker, F.F., Smith, S.L., 2007. Decoupled fresh–saline groundwater circulation of a coastal carbonate aquifer: spatial patterns of temperature and specific electrical conductivity. J. Hydrol. 346, 18–32. doi:10.1016/j.jhydrol.2007.08.013.

Brunner, P., Bauer, P., Eugster, M., Kinzelbach, W., 2004. Using remote sensing to reginalize local precipitation recharge rates obtained from the Chloride Method. J. Hydrol. 294, 241–250.

Butterlin, J., 1958. Reconocimiento geologico preliminary del territorio de Quintana Roo. Bol. Assoc. Mex. Geól. Petroleros 10, 531–570.

Eamus, D., Froend, R., 2006. Groundwater-dependent ecosystems: the where, what and why of GDEs. Aust. J. Botany 54, 91–96.

Effersø, F., Auken, E., Sørensen, K.I., 1999. Inversion of band-limited TEM responses. Geophys. Prospect. 47 (4), 551–564.

Escolero, O.A., Marín, L.E., Steinich, B., Pacheco, J., 2000. Delimitation of a hydrogeological reserve for a city within a karstic aquifer: the Merida, Yucatan example. Landsc. Urban Plan. 51, 53–62.

Fideicomiso para la Promoción Turística de la Rivera Maya, 2004. Estadísticas de Riviera Maya.

Fouke, B.W., Zerkle, A.L., Alvarez, W., Pope, K.O., Ocampo, A.C., Wachtman, R.J., Grajales-Nishimura, J.M., Claeys, P., Fischer, A.G., 2002. Cathodoluminescence petrography and isotope geochemistry of KT impact ejecta deposited 360 km from the Chicxulub crater, at Albion Island, Belize. Sedimentology 49, 117–138.

Gischler, E., Gibson, M.A., Oschmann, W., 2008. Giant Holocene freshwater microbialites, Laguna Bacalar, Quintana Roo, Mexico. Sedimentology 55, 1293–1309.

Goldman, M., Gilad, D., Ronen, A., Melloul, A., 1991. Mapping of seawater intrusion into the coastal aquifer of Israel by the time domain electromagnetic method. Geoexploration 28 (2), 153–174. doi:10.1016/0016-7142(91)90046-.

Gondwe, B.R.N., Hong, S.-H., Wdowinski, S., Bauer-Gottwein, P., 2010. Hydrologic dynamics of the ground-water-dependent Sian Ka'an wetlands, Mexico, derived from InSAR and SAR data. Wetlands 30 (1), 1–13. doi:10.1007/s13157-009-0016-z.

Gondwe, B.R.N., Ottowitz, D., Supper, R., Merediz Alonzo, G., Bauer-Gottwein, P., submitted for publication. Exploring regional-scale preferential flow paths in the karst aquifer of southern Quinana Roo, Mexico.

González-Herrera, R., Sánchez-y-Pinto, I., Gamboa-Vargas, J., 2002. Groundwater-flow modeling in the Yucatan karstic aquifer, Mexico. Hydrogeol. J. 10, 539–552.

Gorohkhovich, Y., Voustianiouk, A., 2006. Accuracy assessment of the processed SRTM-based elevation data by CGIAR using field data from USA and Thailand and its relation to the terrain characteristics. Rem. Sens. Environ. 104, 409–415.

Grajales-Nishimura, J.M., Cedillo-Pardo, E., Rosales-Domínguez, C., Morán-Zenteno, D.J., Alvarez, W., Claeys, P., Ruíz-Morales, J., García-Hernández, J., Padilla-Avila, P., Sánchez-Ríos, A., 2000. Chicxulub impact: the origin of reservoir and seal facies in the southeastern Mexico oil fields. Geology 28 (4), 307–310.

Graniel, C.E., Morris, L.B., Carrillo-Rivera, J.J., 1999. Effects of urbanization on groundwater resources of Merida, Yucatan, Mexico. Environ. Geol. 37 (4), 303–312.

Gunn, J.D., Foss, J.E., Folan, W.J., Carrasco, M.R.D., Faust, B.B., 2002. Bajo sediments and the hydraulic system of Calakmul, Campeche, Mexico. Ancient Mesoam. 13, 297–315.

Hanshaw, B.B., Back, W., 1980. Chemical mass-wasting of the northern Yucatan Peninsula by groundwater dissolution. Geology 8, 222–224.

Hargreaves, G.H., Samani, Z.A., 1985. Reference crop evapotranspiration from temperature. Appl. Eng. Agric. 1 (2), 96–99.

HGG, Denmark, 2001. SEMDI Version 3.1.14.88. Software for Geophysical Inversion of Time-domain Electromagnetic Measurements. HydroGeophysics Group, Aarhus, Denmark.

HGG, Denmark 2007 SiTEM Version 3.1.13.86. Software for Processing of Time-domain Electromagnetic Measurements. HydroGeophysics Group, Aarhus, Denmark.

Hildebrand, A.R., Penfield, G.T., Kring, D.A., Pilkington, M., Camargo, Z.A., Jacobsen, S.B., Boynton, W.V., 1991. Chicxulub crater: a possible Cretaceous/Tertiary boundary impact crater on the Yucatan Peninsula, Mexico. Geology 19, 867–871.

INEGI, 1997. Carta de uso de suelo y vegatación (vegetation map). Recursos electónicos. Escala 1:250,000. Instituto Nacional de Estadística Geogrfía e Informática (INEGI). Shape file.

Jiang, L., Islam, S., 1999. A methodology for estimation of surface evapotranspiration over large areas using remote sensing observations. Geophys. Res. Lett. 26, 2773–2776.

Jiang, L., Islam, S., 2001. Estimation of surface evaporation map over southern Great Plains using remote sensing data. Water Resour. Res. 37 (2), 329–340.

Kenkmann, T., Schönian, F., 2006. Ries and Chicxulub: Impact craters on Earth provide insights for Martian ejecta blankets. Meteor. Planet. Sci. 41 (10), 1587–1603.

Kilroy, G., Coxon, C., Ryan, J., O'Connor, A., Daly, D., 2005. Groundwater and wetland management in the Shannon river basin (Ireland). Environ. Sci. Policy 8, 219–225.

Kiraly, L., 2003. Karstification and groundwater flow. Speleogenesis Evol. Karst Aquifers 1 (3), 26.

Klimchouk, A.B., 1997. The role of karst in the genesis of sulfur deposits, Pre-Carpathian region, Ukraine. Environ. Geol. 31 (1/2), 1–20.

Kocak, G., Buyuksalih, G., Oruc, M., 2005. Accuracy assessment of interferometric digital elevation models derived from the Shuttle Radar Topography Mission X- and C-band data in a test area with rolling topography and moderate forest cover. Opt. Eng. 44 (3), 036201.1–036201.7.

Krause, S., Heathwaite, A.L., Miller, F., Hulme, P., Crowe, A., 2007. Groundwater-dependent wetlands in the UK and Ireland: controls, functioning and assessing the likelihood of damage from human activities. Water Resour. Manage. 21, 2015–2025. doi:10.1007/s11269-007-9192-.

Krekeler, M.P.S., Probst, P., Samsonov, M., Tselepis, C.M., Bates, W., Kearns, L.E., Barry Maynard, J., 2007. Investigations of subsurface flow constructed wetlands and associated geomaterial resources in the Akumal and Reforma regions, Quintana Roo, Mexico. Environ. Geol. 53, 709–726. doi:10.1007/s00254-007-0684-.

Kustas, W.P., Daughtry, C.S.T., Van Oevelen, P.J., 1993. Analytical treatment of the relationships between soil heat flux7net radiation ratio and vegetation indices. Rem. Sens. Environ. 46, 319–330.

Lefticariu, M., Perry, E.C., Ward, W.C., Lefticariu, L., 2006. Post-Chicxulub depositional and diagenetic history of the northwestern Yucatan Peninsula, Mexico. Sediment. Geol. 183, 51–69.

Lesser, J.M., 1976. Estudio hidrogeologico e hidrogeoquimico de la Peninsual de Yucatan. Proyecto Conacyt-NSF 704, Secretaria de Recursos Hidraulicos, Direccion de Geohidrologia y Zonas Aridas, Mexico, 64 p.

Loftus, W.F., Bruno, M.C., Cunningham, K.J., Perry, S., Trexler, J.C., 2001. The ecological role of the karst wetlands of Southern Florida in relation to system restoration. In: Kuniansky, E. (Ed.), Water-Resources Investigations Report 01-4011. US Geological Survey, pp. 8–15.

Lopez-Ramos, E., 1975. Geological summary of the Yucatan Peninsula. In: Nairn, A.E.M., Stehli, F.G. (Eds.), The Ocean Basins and Margins, The Gulf of Mexico and the Caribbean, vol. 3. Plenum Press, NY, USA (Chapter 7).

Marfia, A.M., Krishnamurthy, R.V., Atekwana, E.A., Panton, W.F., 2004. Isotopic and geochemical evolution of ground and surface waters in a karst dominated geological setting: a case study from Belize, Central America. Appl. Geochem. 19, 937–946.

Marín, L.E., 1990. Field investigations and numerical simulation of ground-water flow in the karstic aquifer of northwestern Yucatan, Mexico. PhD thesis, Dept. of Geol., North. Ill. Univ., USA.
Marín, L.E., Steinich, B., Pacheco, J., Escolero, O.A., 2000. Hydrogeology of a contaminated sole-source karst aquifer, Mérida, Yucatán, Mexico. Geofís. Int. 49 (4), 359–365.
Marshall, J.R., Bratton, C., Pope, K.O., Ocampo, A.C., 1998. Diagnostic clast-texture criteria for recognition of impact deposits. In: 29 Annu. Lunar and Planet. Sci. Conf., Houston, TX, USA (Abstract #1134).
Mayr, S.I., Burkhardt, H., Popov, Y., Wittmann, A., 2008. Estimation of hydraulic permeability considering the micro morphology of rocks of the borehole YAXCOPOIL-1 (Impact crater Chicxulub, Mexico). Int. J. Earth Sci. (Geol. Rundsch.) 97, 385–399.
Mazzotti, F.J., Fling, H.E., Merediz, G., Lazcano, M., Lasch, C., Barnes, T., 2005. Conceptual ecological model of the Sian Ka'an Biosphere Reserve, Quintana Roo, Mexico. Wetlands 25 (4), 980–997.
McNeill, J.D., 1986. Geonics EM39 Borehole Conductivity Meter. Theory of Operation. Technical Note TN-20. Geonics Ltd., Ontario, Canada.
Méndez Ramos, R., 1991. Modelo de comportamiento del acuífero de la ciudad de Mérida, Yucatán. Comisión Nacional del Auga, Gerencia Estatal Yucatán, Subgerencia de Administración del Agua, Mérida, Yucatán, Mexico.
Monteith, J.L., 1965. Evaporation and environment. In: Proc. 19th Symp. of the Society of Experimental Biol.. Cambridge University Press, New York.
Moore, Y.H., Stoessell, R.K., Easley, D.H., 1992. Fresh-water/sea-water relationship within a ground-water flow system, northeastern coast of the Yucatan Peninsula. Ground Water 30 (3), 343–350.
Morales Barbosa, J.J., 1992. Los humedales, un mundo olvidado. Series: Sian Ka'an, Introducción a los Ecosistemas de la Península de Yucatan. Amigos de Sian Ka'an A.C. Impresos MARCA, Mérida, Yucatán, Mexico.
Münch, Z., Conrad, J., 2007. Remote sensing and GIS based determination of groundwater dependent ecosystems in the Western Cape, South Africa. Hydrogeol. J. 15, 19–28. doi:10.1007/s10040-006-0125-1.
Munkholm, M.S., Auken, E., 1996. Electromagnetic noise contamination on transient electromagnetic soundings in culturally disturbed environments. J. Environ. Eng. Geophys. 1, 119–127.
NASDA/NASA, 2008. Tropical Rainfall Measuring Mission (TRMM), data products 3B42 and 3B43. TRMM algorithms were developed by the TRMM Science Team. TRMM data were processed by the TRMM Science Data and Information System (TSDIS) and the TRMM Office; archived and distributed by the Goddard Distributed Active Archive Center. TRMM is an international project jointly sponsored by the Japan National Space Development Agency (NASDA) and the US National Aeronautics and Space Administration (NASA) Office of Earth Sciences.
Neuman, B.R., Rahbek, M.L., 2007. Modeling the groundwater catchment of the Sian Ka'an Reserve, Quintana Roo. Assoc. for Mex. Cave Stud. Bull. 18. AMCS Bulletin Publication, Austin, TX, USA.
Ocampo, A.C., Pope, K.O., Fischer, A.G., 1996. Ejecta blanket deposits of the Chicxulub crater from Albion Island, Belize. In: Ryder, G., Fastovsky, D., Gartner, S. (Eds.), The Cretaceous–Tertiary Event and other Catastrophes in Earth History. Geol. Soc. Am. Spec. Pap. 307, pp. 75–88.
Pacheco, J., Marín, L., Cabrera, A., Steinich, B., Escolero, O., 2001. Nitrate temporal and spatial Patterns in 12 water-supply wells, Yucatan, Mexico. Environ. Geol. 40 (6), 708–715.
Parkhurst, D.L., Appelo, C.A.J., 1999. User's guide to PHREEQC (version 2) – a computer program for speciation, reactionpath, 1D-transport, and inverse geochemical calculations. US Geol. Surv. Water-Resour. Investig. Rep. 99-4259.
Perry, E., Swift, J., Gamboa, J., Reeve, A., Sanborn, R., Marín, L., Villasuso, M., 1989. Geologic and environmental aspects of surface cementation, north coast, Yucatan, Mexico. Geology 17, 818–821.
Perry, E.C., Marín, L.E., McClain, J., Velazquez, G., 1995. The Ring of Cenotes (sinkholes) northwest Yucatan, Mexico: its hydrogeologic characteristics and association with the Chicxulub Impact Crater. Geology 23, 17–20.
Perry, E., Velazquez-Oliman, G., Marin, L., 2002. The hydrogeochemistry of the karst aquifer system of the northern Yucatan Peninsula, Mexico. Int. Geol. Rev. 44, 191–221.
Perry, E., Paytan, A., Pedersen, B., Velazquez-Oliman, G., 2009. Groundwater geochemistry of the Yucatan Peninsula, Mexico: constraints on stratigraphy and hydrogeology. J. Hydrol. 367 (1–2), 27–40. doi:10.1016/j.jhydrol.2008.12.026.
Perry, E.C., Velazquez-Oliman, G., Wagner, N., 2010. Groundwater and surface water geochemistry of Cl, SO_4, and Sr in Campeche and southern Quintana Roo. Water Research in México: Scarcity, Degradation, Stress, Conflicts, Management and Policy. Springer, New York.
Pope, K.O., Dahlin, B.H., 1989. Ancient Maya wetland agriculture: new insights from ecological and remote sensing research. J. Field Archeol. 16 (1), 87–106.
Pope, K.O., Ocampo, A.C., Duller, C.E., 1991. Mexican site for K/T impact crater? Nature 351, 105.
Pope, K.O., Ocampo, A.C., Fischer, A.G., Vega, F.J., Ames, D.E., King Jr., D.T., Fouke, B.W., Wachtman, R.J., Kletetschka, G., 2005. Chicxulub impact ejecta deposits in southern Quintana Roo, México, and central Belize. In: Kenkmann, T., Hörz, F., Deutsch, A. (Eds.), Large Meteorite Impacts III. Geol. Soc. Am. Spec. Pap. 384, pp. 171–190.
Priestley, C.H.B., Taylor, R.J., 1972. On the assessment of surface heat flux and evaporation using large scale parameters. Mon. Weather Rev. 100, 81–92.
Rebolledo-Vieyra, M., Urrutia-Fucugauchi, J., Marín, L.E., Trejo-García, A., Sharpton, V.L., Soler-Arechalde, A.M., 2000. UNAM scientific shallow-drilling program of the Chicxulub impact crater. Int. Geol. Rev. 42, 928–940.
Sánchez-Sánchez, O., Islebe, G.A., 2002. Tropical forest communities in south eastern Mexico. Plant Ecol. 158, 183–200.
Schönian, F., Stöffler, D., Kenkmann, T., Wittmann, A., 2004. The fluidized Chicxulub ejecta blanket, Mexico: implications for Mars. Poster. In: 35th Annu. Lunar and Planet. Sci. Conf., League City, TX, USA.
Schönian, F., Tagle, R., Stöffler, D., Kenkmann, T., 2005. Geology of southern Quintana Roo (Mexico) and the Chicxulub ejecta blanket. In: 36th Annu. Lunar and Planet. Sci. Conf., League City, TX, USA (Abstract #2389).
SGM, 2007. Carta geológica de México. Escala 1:2000,000. 6a edición. Servicio Geológico Mexicano (SGM).
Smart, P.L., Beddows, P.A., Coke, J., Doerr, S., Smith, S., Whitaker, F.F., 2006. Cave development on the Caribbean coast of the Yucatan Peninsula, Quintana Roo, Mexico. In: Harmon, R.S., Wicks, C. (Eds.), Perspectives on Karst Geomorphology, Hydrology and Geochemistry – A Tribute Volume to Derek C. Ford and William B. White. Geol. Soc. Am. Spec. Pap. 404, pp. 105–128.
Steinich, B., Marín, L.E., 1996. Hydrogeological investigations in northwestern Yucatan, Mexico, using resistivity surveys. Ground Water 34 (4), 640–646.
Steinich, B., Marín, L.E., 1997. Determination of flow characteristics in the aquifer of the Northwestern Peninsula of Yucatan, Mexico. J. Hydrol. 191, 315–331.
Stisen, S., Sandholt, I., Nørgaard, A., Fensholt, R., Høegh Jensen, K., 2008. Combining the triangle method with thermal intertia to estimate regional evapotranspiration – applied to MSG-SEVIRI data in the Senegal River basin. Rem. Sens. Environ. 112, 1242–1255.
Stoessell, R. et al., no year. Yucatan water chemistry collected by Ronald Stoessell and co-workers. Data from 1980s to 1990s. <http://www.ronstoessell.org/Stoessell_Yucatan.pdf> (accessed January 2009).
Thomas, C., 1999. Aspects hydrologiques du Yucata (Mexique). Karstologia 34, 9–22.
Trimble, 2003 .Trimble Total Control Version 2.73. Software for GPS Data Processing.
Tun-Dzul, F.J., Vester, H., García, R.D., Schmook, B., 2008. Estructura arbórea y variabilidad temporal del NDVI en los "bajos inundables" de la Península de Yucatán, México. Polibotánica 25, 69–90.
USGS, 2006. Shuttle Radar Topography Mission, 3 Arc Second, Finished 2.0. Global Land Cover Facility, University of Maryland, College Park, MD, USA (accessed 15.06.06).
Urrutia-Fucugauchi, J., Marin, L., Trejo-Garcia, A., 1996. UNAM Scientific drilling program of Chicxulub impact structure: evidence for a 300 km crater diameter. Geophys. Res. Lett. 23 (13), 1565–1568.
Urrutia-Fucugauchi, J., Morgan, J., Stöffler, D., Claeys, P., 2004. The Chicxulub scientific drilling project (CSDP). Meteor. Planet. Sci. 39 (5), 787–790.
Urrutia-Fucugauchi, J., Chavez-Aguirre, J.M., Pérez-Cruz, L., De la Rosa, J.L., 2008. Impact ejecta and carbonate sequence in the eastern sector of the Chicxulub crater. CR Geosci. 340, 801–810.
Vacher, H.L., 1988. Dupuit–Ghyben–Herzberg analysis of strip-island lenses. Geol. Soc. Am. Bull. 100 (4), 580–591.
Van der Veer, P., 1977. Analytical solution for steady interface flow in a coastal aquifer involving a phreatic surface with precipitation. J. Hydrol. 34, 1–11.
Wang, K., Li, Z., Cribb, M., 2006. Estimation of evaporative fractin from a combination of day and night land surface temperatures and NDVI: a new method to determine the Priestley–Taylor parameter. Rem. Sens. Environ. 102, 293–305.
Weidie, A.E., 1985. Geology of Yucatan Platform. In: Ward, W.C., Weidie, A.E., Back, W. (Eds.), Geology and Hydrogeology of the Yucatan and Quaternary Geology of Northeastern Yucatan Peninsula. New Orleans Geol. Soc. Publ., New Orleans, LA, USA, pp. 1–12.
Weydahl, D.J., Sagstuen, J., Dick, Ø.B., Rønning, H., 2007. SRTM DEM accuracy assessment over vegetated areas in Norway. Int. J. Rem. Sens. 28 (16), 3513–3527.
Wicks, C.M., Herman, J.S., 1995. The effect of zones of high porosity and permeability on the configuration of the saline–freshwater mixing zone. Ground Water 33 (5), 733–740.
Wohlgemuth, L., Bintakies, E., Kück, J., Conze, R., Harms, U., 2004. Integrated deep drilling, coring, downhole logging, and data management in the Chicxulub Scientific Drilling Project (CSDP), Mexico. Meteor. Planet. Sci. 39 (6), 791–797.
Wolfe, W.J., 1996. Hydrology and tree-distribution patterns of karst wetlands at Arnold Engineering Development Center, Tennessee. Water-Resources Investigations Report 96-4277. United States Geological Survey. Nashville, Tennessee, 50 pp.
Wolff, D.B., Marks, D.A., Amitai, E., Silberstein, D.S., Fisher, B.L., Tokay, A., Wang, J., Pippit, J.L., 2005. Ground validation for the Tropical Rainfall Measuring Mission (TRMM). J. Atmos. Ocean. Technol. 22, 365–380.